Evidence for precursor superconducting pairing above T_c in underdoped cuprates from an analysis of the in-plane infrared response

New Journal of Physics

The open access journal at the forefront of physics

CrossMark

PAPER

Evidence for precursor superconducting pairing above T_c in underdoped cuprates from an analysis of the in-plane infrared response

B Šopík[1], J Chaloupka[1], A Dubroka[1,2], C Bernhard[3] and D Munzar[1,2]

[1] Central European Institute of Technology, Masaryk University, Kamenice 753/5, 62500 Brno, Czech Republic
[2] Department of Condensed Matter Physics, Faculty of Science, Masaryk University, Kotlářská 2, 61137 Brno, Czech Republic
[3] University of Fribourg, Department of Physics and Fribourg Centre for Nanomaterials, Chemin du Musée 3, CH-1700 Fribourg, Switzerland

E-mail: sopik@ceitec.muni.cz and munzar@physics.muni.cz

Keywords: cuprate superconductors, infrared response, precursor superconducting pairing above T_c

Abstract

We performed calculations of the in-plane infrared response of underdoped cuprate superconductors to clarify the origin of a characteristic dip feature which occurs in the published experimental spectra of the real part of the in-plane conductivity below an onset temperature T^{ons} considerably higher than T_c. We provide several arguments, based on a detailed comparison of our results with the published experimental data, confirming that the dip feature and the related features of the memory function $M(\omega) = M_1(\omega) + iM_2(\omega)$ (a peak in M_1 and a kink in M_2) are due to superconducting pairing correlations that develop below T^{ons}. In particular, we show that (i) the dip feature, the peak and the kink of the low-temperature experimental data can be almost quantitatively reproduced by calculations based on a model of a d-wave superconductor. The formation of the dip feature in the experimental data below T^{ons} is shown to be analogous to the one occurring in the model spectra below T_c. (ii) Calculations based on simple models, for which the dip in the temperature range from T_c to T^{ons} is unrelated to superconducting pairing, predict a shift of the onset of the dip at the high-energy side upon entering the superconducting state, that is not observed in the experimental data; (iii) the conductivity data in conjunction with the recent photoemission data (Reber *et al* 2012 *Nat. Phys.* **8** 606, Reber *et al* 2013 *Phys. Rev.* B **87** 060506) imply the persistence of the coherence factor characteristic of superconducting pairing correlations in a range of temperatures above T_c.

1. Introduction

The possible persistence of some form of superconductivity, at least pairing correlations, many tens of K above the bulk superconducting transition temperature T_c in underdoped (UD) cuprate superconductors belongs to the most vividly discussed topics in the field of high-T_c superconductivity, for representative examples of related experimental studies, see [1–15]. Surprisingly high (up to about 100 K above T_c) values of the temperature T^{ons} of the onset of an increase of coherence, presumably due to an onset of precursor superconducting pairing correlations, have been deduced from the data of the c-axis infrared response of UD YBa$_2$Cu$_3$O$_{7-\delta}$ (Y-123) [6]. More recently, the interpretation of the T^{ons} scale in terms of a precursor superconductivity has been supported by results obtained by Uykur and coworkers [7]. They address the persistence of the superfluid density above T_c and the impact of Zn doping on T^{ons} (T^p in the notation of [7]). This interpretation, however, has not yet been commonly accepted. Two reasons are: (i) the c-axis response of Y-123 is a fairly complex quantity due to the specific bilayer structure of this compound. Its interpretation therefore requires a detailed understanding of the c-axis electrodynamics of the bilayer compounds [16–23]. (ii) UD cuprates are known to exhibit ordered phases distinct from superconductivity, in particular, charge modulations have been reported [24, 25], that set in at temperatures comparable to T^{ons}. This has fueled speculations that the T^{ons} scale is determined by an order

different from and possibly competing with superconductivity rather than by pairing correlations themselves. In this context, it is of high importance to identify manifestations of the increase of coherence below T^{ons} in the in-plane response, a quantity revealing aspects of the electronic structure complementary to those manifesting themselves in the *c*-axis response, and to ascertain their relation to superconducting pairing correlations.

It has been already shown [6] that the real part of the in-plane infrared conductivity of UD Y-123 changes at T^{ons} in a way similar to that of an optimally doped (OPD) superconductor at T_c: a dip-like feature with a minimum around 400 cm^{-1} begins to form and this is accompanied by a pronounced spectral weight shift from the dip region to very low frequencies (below ca 200 cm^{-1}). The focus, however, has been on qualitative aspects of the relevant spectral weight shifts, and the related spectral structures have not been addressed. Here we concentrate on three prominent spectral features that develop below T^{ons}: the onset of the dip at the high energy side, the corresponding peak in the spectra of the real part of the memory function and the corresponding kink in the spectra of the imaginary part of the memory function. Our analysis involves comparisons of the data of two representative UD cuprates with those of OPD ones and with results of our calculations employing approaches ranging from the Allen's theory to the fully selfconsistent generalized Eliashberg theory. It provides evidence that the features are due to superconducting pairing correlations, and the scale T^{ons} due to a precursor superconducting pairing phase rather than to an ordered state unrelated to superconductivity.

Recall that T^{ons} is significantly lower than $T^\star$, the temperature of the onset of the pseudogap as seen, e.g., in the planar copper Knight shift [26], in the *c*-axis conductivity [27–30], in the intrinsic tunnelling [31, 32], in the angular resolved photoemission spectra of the antinodal region of the Brillouin zone [33] etc. For UD Y-123 with 10% doping $T^\star > 300$ K [6, 7, 28, 29, 34], while $T^{\text{ons}} \approx 170$ K [6, 7]. The pseudogap region of the phase diagram of the cuprates located between the T_c line and the $T^\star$ line involves two distinct types of electronic correlations: the correlations setting on at $T^\star$, on the one hand, cause a depletion of the electronic density of states at low energies and they seem to compete with superconductivity [30]. The correlations setting on at T^{ons}, on the other hand, bring about an increase of coherence of the electronic states manifesting themselves both in the out-of plane and in the in-plane response [6].
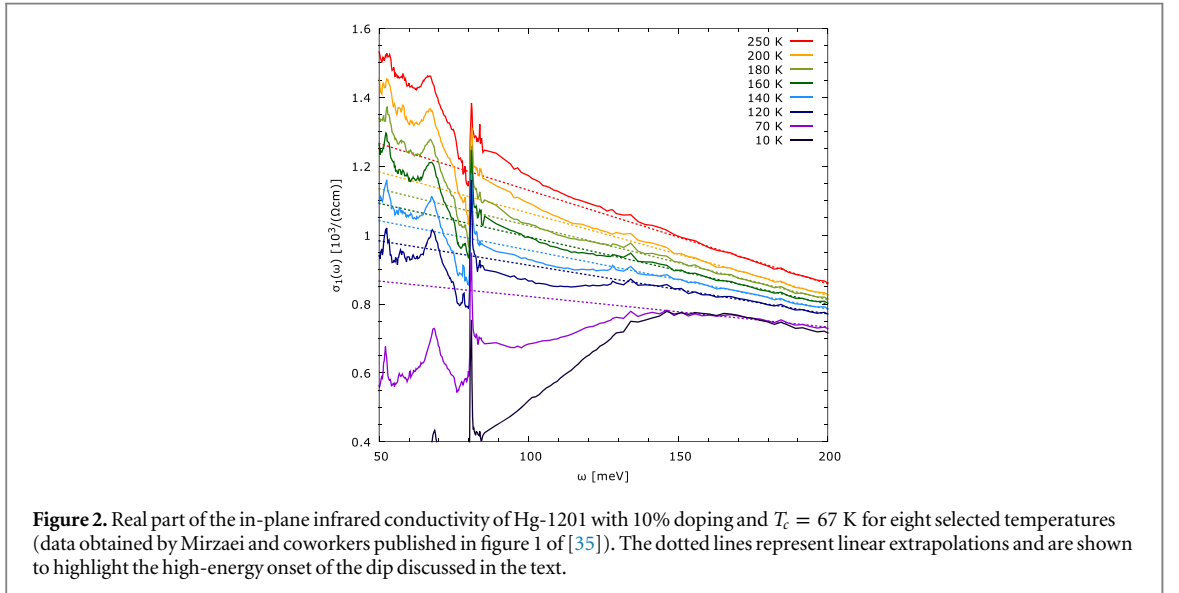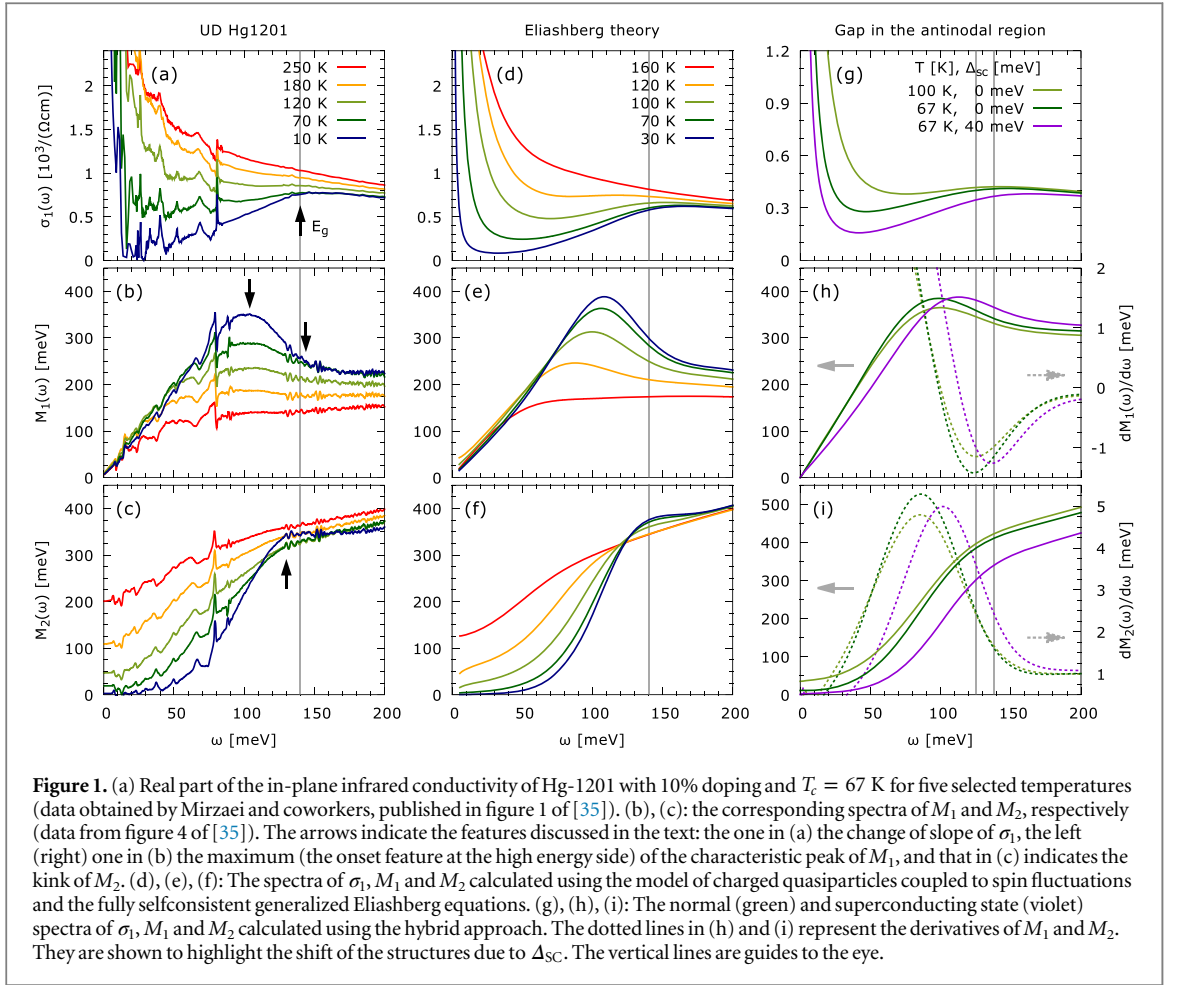
The paper is organized as follows. In section 2 we summarize the relevant aspects of the experimental infrared data. As examples we use the published data of UD HgBa$_2$CuO$_{4+\delta}$ (Hg-1201) [35] and Y-123 [6, 36]. At the end of the section, the data are compared with the published ones of OPD cuprates. In section 3 we present and discuss results of our calculations aiming to clarify the origin of the spectral structures. First (in subsection 3.1), we focus on the spectra calculated using the Eliashberg theory. We put emphasis on the similarity between the low-temperature (*T*) data and the low-*T* calculated spectra and on the similarity between the onset of the spectral structures below T^{ons} in UD cuprates and that below T_c in the calculated spectra. In subsection 3.2, the data are discussed in terms of the frequently used extended Allen's theory (EAT) [36–39]. It is highlighted that the assumption of a superconductivity unrelated gap in the density of states in the temperature range $T_c < T < T^{\text{ons}}$ leads to inconsistencies with the data. In particular, we show that it leads to a clear shift of the high energy onset of the dip upon entering the superconducting state, that is not observed in the experimental data. This applies also to simple models, where the dip in the temperature range $T_c < T < T^{\text{ons}}$ is attributed solely to an electron–boson coupling and the temperature dependence of the Fermi and Bose factors. Finally, in subsection 3.3, we present and discuss results of our calculations of the optical spectra, using as inputs recently published properties of the quasiparticle spectral function obtained from the photoemission data by means of analyzing the tomographic density of states [10]. A short summary and conclusions are given in section 4.

2. Relevant aspects of the published experimental data

The dip feature in the spectra of the real part σ_1 of the infrared conductivity σ will be illustrated with the recently published data of UD HgBa$_2$CuO$_{4+\delta}$ (Hg-1201) with 10% doping and $T_c = 67$ K [35]. Also discussed will be the related structures of the memory function $M(\omega) = M_1(\omega) + M_2(\omega)$, defined by $\sigma(\omega) = i\varepsilon_0 \omega_{\text{pl}}^2 \hbar / [M(\omega) + \omega]$ [40] and connected to the so called optical selfenergy $\sum^{\text{opt}}(\omega)$ by $\sum^{\text{opt}}(\omega) = -M(\omega)/2$. Here ω_{pl} is the plasma frequency. The data of UD Hg-1201 of [35] are similar to the earlier published ones of UD Y-123 [6, 36], but a much more detailed temperature dependence is reported and some spectral features are sharper than in Y-123.

Figure 1 shows, in part (a), a selection of the spectra of σ_1 of Hg-1201 from figure 1 of [35], and, in parts (b) and (c), the corresponding spectra of M_1 and M_2 from figure 4 of [35]. The low-temperature spectra of σ_1 contain the δ-peak at $\omega = 0$ (not shown in the figure) corresponding to the loss-free contribution of the superconducting condensate, a narrow low-energy component corresponding to residual quasiparticles, and a deep and broad minimum around 30 meV (see, e.g., the 10 K line in figure 1(a)). This is followed by a broad region of an approximately linear increase terminating at $E_g \approx 140$ meV, where the slope of the spectrum

Figure 1. (a) Real part of the in-plane infrared conductivity of Hg-1201 with 10% doping and $T_c = 67$ K for five selected temperatures (data obtained by Mirzaei and coworkers, published in figure 1 of [35]). (b), (c): the corresponding spectra of M_1 and M_2, respectively (data from figure 4 of [35]). The arrows indicate the features discussed in the text: the one in (a) the change of slope of σ_1, the left (right) one in (b) the maximum (the onset feature at the high energy side) of the characteristic peak of M_1, and that in (c) indicates the kink of M_2. (d), (e), (f): The spectra of σ_1, M_1 and M_2 calculated using the model of charged quasiparticles coupled to spin fluctuations and the fully selfconsistent generalized Eliashberg equations. (g), (h), (i): The normal (green) and superconducting state (violet) spectra of σ_1, M_1 and M_2 calculated using the hybrid approach. The dotted lines in (h) and (i) represent the derivatives of M_1 and M_2. They are shown to highlight the shift of the structures due to Δ_{SC}. The vertical lines are guides to the eye.

Figure 2. Real part of the in-plane infrared conductivity of Hg-1201 with 10% doping and $T_c = 67$ K for eight selected temperatures (data obtained by Mirzaei and coworkers published in figure 1 of [35]). The dotted lines represent linear extrapolations and are shown to highlight the high-energy onset of the dip discussed in the text.

changes, see the arrow in figures 1(a) and figure 2 . This change of slope will be called the high energy onset of the dip (HEOD). It is associated with a local maximum at a slightly higher energy. The HEOD is further accompanied by a characteristic peak in the spectra of M_1 with an onset feature at the high energy side (around E_g), and a kink in those of M_2, see the arrows in figures 1(b) and (c). All the three features are well known from earlier infrared studies [28, 36, 38, 39, 41]. What has, however,—to the best of our knowledge—not yet been recognized, is the fact that they start to form close to the temperature T^{ons} of [6].

This will be discussed below. We focus on σ_1 first. The 70 K and 120 K spectra in figure 1(a) display a clear HEOD at an energy close to E_g, see also figure 2. The 250 K spectrum, on the other hand, does not display any such feature in the relevant spectral range. It can be seen in figure 1 of [35], see also figure 2, that the dip feature vanishes at a temperature higher than 160 K but $\lesssim 200$ K, close to the maximum T^{ons} of [6] (180 K). Based on this finding and the earlier observations of [6] we assume that the temperature scale of the dip coincides with the earlier established T^{ons} of [6] and T^p of [7] and denote it by T^{ons}. The T-dependence of the characteristic peak in the spectra of M_1 is similar: at 70 K and 120 K it is still very pronounced and almost at the same location as at low temperatures, at 250 K a clear maximum is not evident (see also figure 4 of [35]; the remaining very weak band in the 90–130 meV range seems to be of different origin, perhaps related to the sharp structure at ca 80 meV). Note that the onset feature at the high energy side of a similar peak occurring in the case of UD Y-123 has already been reported to vanish around 170 K [36], see discussion of figure 7 in [36]. Next we address the T-dependence of the kink in the spectra of M_2. At low temperatures the feature is very sharp (note that the 10 K spectrum overshoots the 70 K one). It gets less sharp around T_c but persists, at approximately the same energy, up to much higher temperatures, see figure 4 of [35]. In the 120–200 K range, it transforms into a smoother onset at a lower energy due to the presence of the relatively narrow low energy component of σ_1, that can be seen in figure 2, rather than to the HEOD. Note finally that the onset of the features is very likely connected with a transition to a purely quadratic T-dependence of the dc resistivity occurring slightly above 200 K [35] and with the appearance below about 200 K of a Fermi-liquid like scaling of $M(\omega)$ [35].

In OPD materials, a dip feature in $\sigma_1(\omega)$ terminated by a local maximum, a peak in $M_1(\omega)$ and a kink in $M_2(\omega)$, similar to those discussed above, set in at T_c (or very slightly above T_c). For representative examples, see [42–45]. These features of OPD materials are clearly caused by superconductivity, since they develop in parallel with the formation of the loss-free contribution to $\sigma(\omega)$ of the superconducting condensate, involving the δ-peak at $\omega = 0$ in $\sigma_1(\omega)$: the δ-peak collects the spectral weight lost by the formation of the dip. It appears, that the three features of OPD materials, that set in at T_c and are due to superconductivity, continuously transform into those of the UD ones, setting in at T^{ons}. This is a strong phenomenological argument in favor of the superconducting pairing-based interpretation of the three features and the precursor superconducting pairing based interpretation of the T^{ons} scale.

3. Results and discussion

3.1. Response functions calculated using the Eliashberg theory, comparison with the data

Recall that many properties of OPD cuprate superconductors, including superconductivity, can be (at least qualitatively) understood in terms of (various versions of) the model, where charged planar quasiparticles are coupled to spin fluctuations. For reviews, see [46–51]. In particular, the low-T spectra of σ_1 in the superconducting state have been well reproduced [52–55] using a phenomenological version of the model, where the spin fluctuation spectrum $\chi(\nu, \mathbf{q})$ is approximated by a narrow (in ν) mode centered at the frequency of the magnetic resonance. By including a continuum contribution to $\chi(\nu, \mathbf{q})$ and performing the calculations at the fully selfconsistent generalized Eliashberg level, almost quantitative agreement with the data can be achieved [56], see also [57]. In the following we demonstrate that even the low-T experimental spectra of UD Hg-1201 can be approximately reproduced using the generalized Eliashberg approach formulated in [56]. In order to avoid any misunderstanding, we emphasize here that it is not the purpose of the present paper to advocate a very specific model. There are only two ingredients of the model, that are really essential for our conclusions: the superconducting order of d-wave symmetry and the relatively strong coupling between charge carriers and bosonic excitations (not necessarily spin fluctuations), whose spectral density is peaked around 40–50 meV. Other ingredients—the presence of a tail of the spectrum of the bosonic excitations ranging to high energies, the full selfconsistency etc.—help to reproduce the low temperature data quantitatively.

We begin with a brief description of the computational approach, details can be found in appendix A. The generalized Eliashberg equations (see, e.g., [58]) can be written as

$$\hat{\Sigma}\left(\mathrm{i}\omega_n, \mathbf{k}\right) = \frac{g^2}{\beta N} \sum_{m,\mathbf{q}} \chi\left(\mathrm{i}\nu_m, \mathbf{q}\right) \hat{G}\left(\mathrm{i}\omega_n - \mathrm{i}\nu_m, \mathbf{k} - \mathbf{q}\right), \tag{1}$$

where $\hat{\Sigma}$ is the matrix selfenergy that can be expressed in terms of the Pauli matrices as $\hat{\Sigma} = \Sigma^{(0)}\hat{\tau}_0 + \Sigma^{(3)}\hat{\tau}_3 + \Sigma^{(1)}\hat{\tau}_1$, $\hat{G} = G^{(0)}\hat{\tau}_0 + G^{(3)}\hat{\tau}_3 + G^{(1)}\hat{\tau}_1$ is the renormalized quasiparticle propagator,

$$\hat{G}^{-1}\left(\mathrm{i}\omega_n, \mathbf{k}\right) = \mathrm{i}\omega_n\hat{\tau}_0 - [\epsilon(\mathbf{k}) - \mu]\hat{\tau}_3 - \hat{\Sigma}\left(\mathrm{i}\omega_n, \mathbf{k}\right), \tag{2}$$

$\chi(\mathrm{i}\nu_m, \mathbf{q})$ is the Matsubara counterpart of the the spin susceptibility, g is the coupling constant, $\mathrm{i}\omega_n$ and $\mathrm{i}\nu_m$ are the fermionic and bosonic Matsubara energies, respectively. The equations have been solved on the real axis using spectral representations of $\hat{G}$ and χ. We have used the same form of the input spin susceptibility as in our

previous studies [55] and [56]. It contains a narrow (in frequency) mode centered at the frequency of the magnetic resonance and a component approximating the spin-fluctuation continuum. The corresponding formulas, the values of all input parameters, providing the values of T_c and $\Delta_{\max}$ of 133 K and 45 meV, respectively, and some intermediate results are given in appendix A. Here $\Delta_{\max}$ is the maximum value of the superconducting gap of $d_{x^2-y^2}$ symmetry. The high value of T_c is not surprising considering the observation of [59] that the value of the spin-fermion coupling constant providing the best fit of the nodal kink in UD Y-123 yields a high T_c value of 175 K.

Finally, after obtaining the selfconsistent solution of the generalized Eliashberg equations, the optical conductivity was calculated using the formula

$$\sigma_{xx}(\omega) = \frac{ie^2 N_p}{\hbar d} \frac{\left[-K_{xx} + \Pi_{xx}(\omega) \right]}{\omega + i0}. \tag{3}$$

Here d is the c-axis lattice parameter ($d = 9.52$ Å for Hg-1201, $d = 11.65$ Å for Y-123), N_p is the number of CuO_2 planes within a unit cell ($N_p = 1$ for Hg-1201, $N_p = 2$ for Y-123) and ω is here in units of energy. The expressions K_{xx} and $\Pi_{xx}(\omega)$ in the numerator provide the diamagnetic and paramagnetic contributions to the optical conductivity, respectively. Both can be expressed in terms of the matrix quasiparticle spectral function $\hat{A} = A^{(0)}\hat{\tau}_0 + A^{(3)}\hat{\tau}_3 + A^{(1)}\hat{\tau}_1$ defined by $\hat{A}(\omega, \mathbf{k}) = -2\,\mathrm{Im}\{\hat{G}(\omega + i0, \mathbf{k})\}$. The diamagnetic term is given by the following formula (exact)

$$K_{xx} = -\frac{1}{N}\sum_{\mathbf{k}} \frac{\partial^2 \epsilon(\mathbf{k})}{\partial(k_x a)^2}\left[1 - \int_{-\infty}^{\infty} \frac{dE}{2\pi} A^{(3)}(E, \mathbf{k})\tanh\frac{\beta E}{2} \right]. \tag{4}$$

The paramagnetic term is given by the current–current correlation function and can be expressed (in terms of $\hat{A}$) only approximately. The most frequently used approximation, employed also in our calculations, completely neglects vertex corrections and leads to the following formula for the imaginary part Π_{xx}'' of Π_{xx}:

$$\Pi_{xx}''(\omega) = -\frac{1}{2N}\sum_{\mathbf{k}}\left(\frac{\partial\epsilon(\mathbf{k})}{\partial k_x a} \right)^2$$
$$\times \int_{-\infty}^{\infty} \frac{d\nu}{2\pi}\,\mathrm{Tr}\left\{ \hat{A}(\nu, \mathbf{k})\hat{A}(\nu + \omega, \mathbf{k}) \right\}[f(\nu) - f(\nu + \omega)]. \tag{5}$$

The real part Π_{xx}' of Π_{xx} was obtained using the Kramers–Kronig transformation. Note that the expression on the right hand side of equation (3) includes the contribution of the condensate, the superfluid plasma energy $\hbar\omega_{\mathrm{pl,sc}}$ is given by

$$\hbar^2\omega_{\mathrm{pl,sc}}^2 = \frac{e^2 N_p}{d\epsilon_0}\left[\Pi_{xx}'(0) - K_{xx} \right]. \tag{6}$$

In order to assess the validity of the approximation of equation (5), we have also evaluated Π_{xx} using the gauge invariant approach of [56], where an important class of vertex corrections is included. The corrections modify the spectra of Π_{xx}'' only slightly, the only significant problem of the approximation being an underestimation of the total spectral weight at finite frequencies and $|\Pi_{xx}'(0)|$ by ca 8%. For the normal state, this leads to the presence of a small unphysical singular component. In order to avoid the problem, we have replaced K_{xx} with $\Pi_{xx}'(0)$ in the normal state calculations. For temperatures below T_c, we have set $K_{xx} = \Pi_{xx}'(0)$ [140 K]. The corresponding value of the (total) plasma energy $\hbar\omega_{\mathrm{pl}}$ is 1.95 eV.

For future reference, we provide here also the formula for the real part $\sigma_1(\omega)$ of $\sigma_{xx}(\omega)$ resulting from equation (5):

$$\sigma_1(\omega) = \frac{e^2 N_p}{d\hbar\omega}\frac{1}{N}\sum_{\mathbf{k}}\left(\frac{\partial\epsilon}{\partial(k_x a)} \right)^2 \int_{-\infty}^{\infty} \frac{d\nu}{2\pi}\{ A(\nu, \mathbf{k})A(\nu + \omega, \mathbf{k})$$
$$+ A^{(1)}(\nu, \mathbf{k})A^{(1)}(\nu + \omega, \mathbf{k}) \}[f(\nu) - f(\nu + \omega)], \tag{7}$$

where $A(\nu, \mathbf{k}) = A^{(0)}(\nu, \mathbf{k}) + A^{(3)}(\nu, \mathbf{k})$ is the usual spectral function. The normal state version of the formula reads
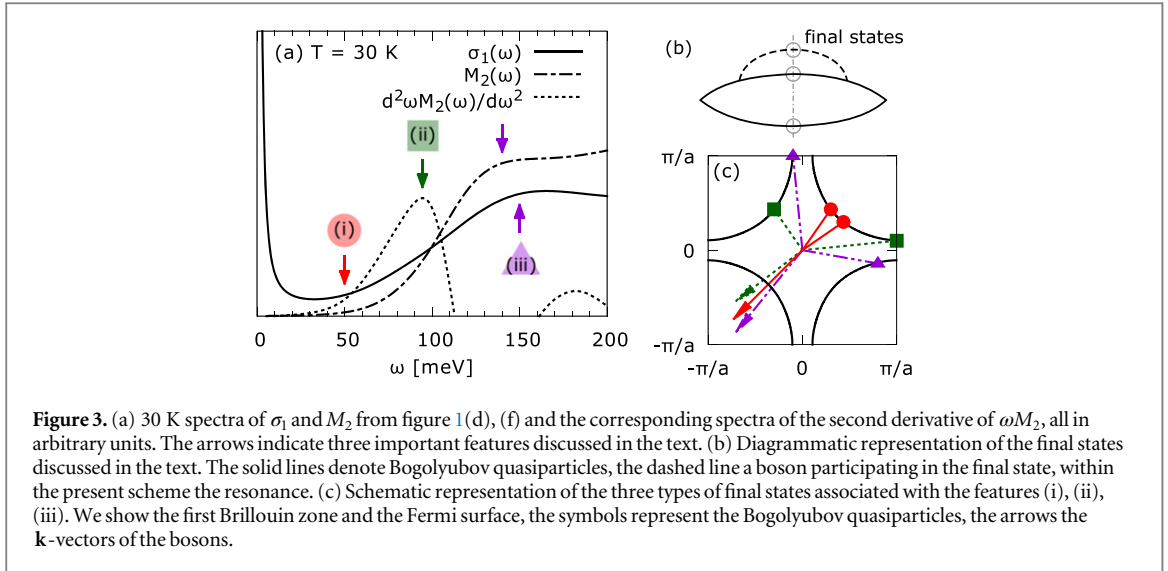
Figure 3. (a) 30 K spectra of σ_1 and M_2 from figure 1(d), (f) and the corresponding spectra of the second derivative of ωM_2, all in arbitrary units. The arrows indicate three important features discussed in the text. (b) Diagrammatic representation of the final states discussed in the text. The solid lines denote Bogolyubov quasiparticles, the dashed line a boson participating in the final state, within the present scheme the resonance. (c) Schematic representation of the three types of final states associated with the features (i), (ii), (iii). We show the first Brillouin zone and the Fermi surface, the symbols represent the Bogolyubov quasiparticles, the arrows the **k**-vectors of the bosons.

$$\sigma_1(\omega) = \frac{e^2 N_p}{d\hbar\omega} \frac{1}{N} \sum_{\mathbf{k}} \left(\frac{\partial \epsilon}{\partial(k_x a)} \right)^2$$
$$\times \int_{-\infty}^{\infty} \frac{d\nu}{2\pi} A(\nu, \mathbf{k}) A(\nu + \omega, \mathbf{k}) [f(\nu) - f(\nu + \omega)]. \tag{8}$$

Figures 1(d)–(f) show the calculated spectra of σ_1, M_1, and M_2, respectively. Note the agreement between the low-T spectra and the low-T data shown in figures 1(a)–(c). The structures of σ_1 and M_2, in particular a weak onset around the energy of the resonance mode $\hbar\omega_0$ (here 50 meV), and the HEOD of σ_1 and the corresponding kink of M_2 at $\approx \hbar\omega_0 + 2\Delta_{max}$, can be interpreted along the lines of the earlier theoretical studies [55, 56]. For the convenience of the reader, the interpretation is summarized in the following paragraph.

Figure 3(a) shows the 30 K spectra of σ_1 and M_2 from figures 1(d) and (f) and the corresponding spectra of the second derivative of ωM_2, all in arbitrary units. The arrows indicate three important features, occuring also in the experimental spectra of OPD cuprates, whose interpretation was presented in [55, 56]: (i) a weak onset of σ_1 and M_2 around the energy $\hbar\omega_0$ of the bosonic mode (within the present context the magnetic resonance) [43, 44, 52, 55, 56]. (ii) A maximum of the second derivative of ωM_2 [60] at approximately $\hbar\omega_0 + \Delta_{max}$ [53, 55, 56]. (iii) A local maximum of σ_1 at E_g with E_g approximately equal or slightly above $\hbar\omega_0 + 2\Delta_{max}$ [43, 44, 54, 56], associated with the HEOD, and the corresponding kink of M_2. At the simplest relevant perturbative level (Bogolyubov quasiparticles of a d-wave superconductor coupled to bosons), the basic infrared active final states consist of two Bogolyubov quasiparticles and the bosonic mode, see figure 3(b). Final states consisting of two Bogolyubov quasiparticles are not infrared active in the clean limit. The features (i), (ii), and (iii) are due, as detailed in [55, 56], to the appearance above the characteristic energies ($\hbar\omega_0, \hbar\omega_0 + \Delta_{max}$, $\hbar\omega_0 + 2\Delta_{max}$) of final states consisting of (i) two near nodal (Bogolyubov) quasiparticles and the bosonic mode, (ii) a near nodal quasiparticle, an antinodal quasiparticle and the mode, and (iii) two antinodal quasiparticles and the mode. Above $\hbar\omega_0 + 2\Delta_{max}$, the density of available final states saturates. A schematic representation of the three types of final states, associated with the features (i), (ii), and (iii) is presented in figure 3(c).

The relation $E_g \approx 2\Delta_{max} + \hbar\omega_0$ [54–56] allows for a quantitative consistency check. The value of E_g of UD Hg-1201 of 140 meV is indeed approximately consistent with the available experimental values of $\hbar\omega_0$ and Δ_{max} ($\hbar\omega_0 \approx 50$ meV [61], $\Delta_{max} \approx 39$ meV [62], $\Delta_{max} \approx 45$ meV [63]). Recently, a similar consistency check has been applied to the infrared data of OPD $Bi_2Sr_2CaCu_2O_{8+\delta}$ (Bi-2212) by Homes and coworkers [64]. To conclude, the low-T infrared spectra of UD Hg-1201 are consistent with a well established model of a d-wave superconductor.

Next we address the T-dependence of the model spectra. It can be seen in figures 1(d)–(f) that the three important features (the dip of σ_1, the maximum of M_1 and the M_2 kink) develop below T_c in the same fashion as in the data of OPD materials [42–45]. In particular, the σ_1 dip forms already close to T_c. What we would like to highlight here is that not only the T dependence of the data of OPD cuprates but also that of the UD is similar to the model spectra, compare figures 1(a)–(c) with figures 1(d)–(f). Note that the development of the dip in the UD Hg-1201 below $T^{ons} \approx 180$ K is analogous to that of the model spectra below T_c: somewhat below T^{ons}/T_c a characteristic change of slope appears in $\sigma_1(\omega)$, with decreasing T its energy approaches E_g and the minimum at low energies and the characteristic maximum around E_g are forming. In the model spectra, the energy scale of

the dip develops more gradually than in the data. This difference is most likely due to the mean field character of the model. The similarity between the T-dependence of the data below T^{ons} and that of the model spectra below T_c provides a further support for the interpretation of the T^{ons} scale in terms of a precursor superconducting pairing state, for which T^{ons} corresponds to the mean field transition temperature.

Admittedly, the mean field model does not reproduce the low-energy part of the data above T_c. The calculated spectra of σ_1 at 70 K, 100 K, and 120 K contain a δ function at $\omega = 0$ (not shown), which is not present in the corresponding experimental spectra. In addition, the calculated spectra of M_2 at 70 K, 100 K, and 120 K display a more gradual increase with increasing frequency than the experimental ones, that satisfy the Fermi-liquid like scaling, $M_2(\omega, T) \sim \xi^2$, with $\xi = \sqrt{(\hbar\omega)^2 + (p\pi k_B T)^2}$ and $p = 1.5$ [35]. In our opinion, these discrepancies are due to the presence of strong fluctuations which suppress the long range phase coherence in the temperature range from T_c to T^{ons}. An adequate microscopic description of the spectra in this temperature range must include the fluctuating condensate and/or a contribution of uncondensed pairs, and the coupling between the former and the thermally excited quasiparticles. Note, however, that in the frequency range around the HEOD, the impact of the fluctuations on the spectral features can be expected to be of less importance. For completeness, the T-dependence of the contribution of the condensate/fluctuating condensate in UD cuprates will be qualitatively discussed below. At low temperatures, the response of the condensate is represented by the δ-peak at $\omega = 0$ in $\sigma_1(\omega)$. When going from $T = 0$ to T_c, the spectral weight of the δ-peak decreases, which is compensated by the filling in of the gap [65, 66]. At T_c, the δ-peak vanishes but the superfluid does not, merely its long range phase coherence has been lost [67]. Simultaneously, the superfluid acquires a finite phasecorrelation time τ, probably due to a random motion of unbound thermally excited vortices, and the δ-peak is replaced with a Drude peak of finite width $\sim 1/\tau$ [68, 69] that cannot be easily distinguished from the response of thermally excited quasiparticles.

For our considerations on the origin of the three spectral structures, it is very important that the THz experiments [68] have clearly confirmed the presence of a fluctuating condensate at T_c and at temperatures slightly higher than T_c. For a slightly UD epitaxial film of Bi-2212 with $T_c = 74$ K, the reported value of the fluctuating condensate density at T_c ($T_c + 5$ K) is ca 35% (25%) of that at low temperatures (see the T_θ^0 line in figure 4 of [68]). Based on this observation only, it can be expected, with a high degree of certainty, that the more strongly UD Hg-1201 sample of [35] will be, at temperatures not much higher than $T_c = 67$ K, e.g., at 70 K, in a fluctuating state with a considerable value of the fluctuating condensate density and the magnitude of the superconducting gap not very different from the low-T one. And, importantly, there is no clear qualitative difference between the 70 K experimental data of [35] and the 80 K, 90 K and 100 K ones.

When going from T_c to higher temperatures, the spectral weight of the fluctuating condensate (i.e., that of the corresponding narrow Drude peak) decreases further [68], in parallel with the filling in of the gap. At the same time, τ decreases dramatically [68], so that for T above ca $T_c + 20$ K, the contribution of the fluctuating condensate could not be distinguished from that of normal state electrons [68, 69], see also [70]. It has remained an open question [71], whether at higher temperatures the fluctuating condensate is simply absent or merely unobservable by the THz techniques, while manifesting itself in the Nernst and diamagnetic response [1–3]. The data reported by Mirzaei and coworkers clearly show that the process of filling in the gap, very similar to that of OPD cuprates or that of a model d-wave superconductor (the similarity has been demonstrated in the present study), continues up to T^{ons}, and the spectral weight comes from the lowest frequencies ($\omega < 20$ meV). For these reasons we suspect that the partially condensed and/or uncondensed pairs persist up to T^{ons} providing a low-energy component of $\sigma(\omega)$. This issue will be addressed again at the end of section 3.3. Finally, we note that the precursor phenomena discussed above may be strongly influenced by a spatial inhomogeneity of the superconducting order [4, 72].

In our calculations, fluctuations of the condensate have not been included. There is no established way of doing this in conjunction with a retarded interaction, which is needed for a description of the infrared response. Previous attempts are limited to phenomenological models (e.g., [73]) and models involving a nonretarded interaction (e.g., [74]). Manske and coworkers [75] have used the fluctuation exchange approximation combined with results of the Kosterlitz–Thouless theory and thermodynamic considerations based on the Ginzburg–Landau theory to estimate the difference between T_c and the mean field transition temperature ($T_c^\star$) and have confirmed the claim of [67] that in UD cuprates T_c is considerably lower than $T_c^\star$. This approach, however, cannot be easily extended towards calculations of the optical conductivity in the fluctuating state.

The calculations also do not include the pseudogap setting on at $T^\star$ ('antinodal pseudogap'). Its opening can be expected to influence the in-plane conductivity in two different ways: (a) directly, by modifying the contribution to σ_1 of the antinodal region, that is approximately determined by the corresponding contribution to the sum over **k** on the right hand side of equation (8). (b) Indirectly, through a renormalization of near nodal quasiparticles, caused by a nodal–antinodal boson assisted scattering. The former contribution can be expected to be small since in moderately UD cuprates the pseudo-gapped region of the Brillouin zone around the

antinode is relatively small [33, 76] and, in addition, the magnitude of the corresponding vertex ($\sim \frac{\partial \epsilon}{\partial(k_x a)}$) is small. The mechanism (b) may influence the spectra significantly. The large difference between $T^\star$ and T^{ons}, however, indicates, that the dip feature in the spectra of σ_1 is not caused by the antinodal pseudogap. In the following subsection we further demonstrate, using the EAT, that the feature is unlikely to be caused by an order setting on at T^{ons} and unrelated to superconducting pairing.

3.2. Analysis of the above T_c data based on the EAT, problems of interpretations not involving pairing

The normal state (i.e., above T_c) spectra of M_1 and M_2 of UD Y-123 and $Bi_2Sr_2CaCu_2O_{8+\delta}$ (Bi-2212) have been previously successfully fitted and interpreted in terms of the phenomenological EAT [36–39]. This is based on two implicit assumptions: (i) the in-plane response is dominated by the contribution of near nodal quasiparticles; (ii) the dominant part of the renormalization of these quasiparticles comes from a nodal–antinodal boson assisted scattering, the antinodal region being gapped. The essential inputs are a function $\alpha^2 F(\nu)$ describing bosonic excitations and a density of states $N(\omega)$ displaying the antinodal gap, whose physical origin is not specified. Here we provide two indications that the gap captured by the EAT based fits is likely related to superconducting pairing.

(i) We have fitted the Hwang's data of UD Y-123 reported in [36] using the formulas of the EAT, i.e., the Allen's formula [77, 78]

$$\sigma(\omega) = \frac{i\epsilon_0}{\hbar} \frac{\omega_{\text{pl}}^2}{\omega} \int_{-\infty}^{\infty} d\epsilon \frac{f(\epsilon) - f(\omega + \epsilon)}{\omega - \Sigma(\omega + \epsilon) + \Sigma^\star(\omega)}, \tag{9}$$

where ω and ω_{pl} are in units of energy, the formula for the imaginary part Σ_2 of the retarded selfenergy Σ proposed in [37]

$$\Sigma_2(\omega) = -\pi \int_0^\infty d\nu \alpha^2 F(\nu) \{ N(\omega - \nu)[b(\nu) + 1 - f(\omega - \nu)] \\ + N(\omega + \nu)[b(\nu) + f(\omega + \nu)] \}, \tag{10}$$

and

$$\Sigma_1(\omega) = -\frac{1}{\pi} \mathcal{P} \int_{-\infty}^{\infty} d\nu \frac{\Sigma_2(\nu)}{\omega - \nu}. \tag{11}$$

We have achieved a degree of agreement comparable to that of previous studies (e.g., that of [39]). In the above equations, $b(\nu)$ and $f(\omega)$ are the Fermi and the Bose functions, respectively. Our ansatz for $\alpha^2 F(\nu)$, the one for $N(\omega)$, and a detailed description of our fits can be found in appendix B.

The important findings are: (a) while the presence of the density of states gap is needed to achieve a high quality fit for temperatures well below T^{ons}, it is not essential for temperatures higher than T^{ons}. For the latter temperatures (and not for the former, see appendix C), the simple Allen's theory [77, 78], as used in [79, 80], appears to be sufficient. The characteristic temperature of the sharp gap of the EAT based fits is thus T^{ons} rather than the pseudogap temperature $T^\star$. (b) The opening of the gap in the density of states causes a spectral weight shift from the dip region to low frequencies, the same effect as expected for a precursor superconducting pairing state.

(ii) Assuming that the physics at $T_c < T < T^{\text{ons}}$ is unrelated to superconducting pairing, we arrive at a contradiction with the experimental data, as outlined below. Starting from the above assumption, the opening of the superconducting gap in the near nodal region below T_c can be expected to give rise to a blue shift of the structures established above T_c. This blue shift occurs indeed in the calculated spectra, see the discussion below, but is not seen in the experimental data. Figure 1(g) shows the normal (100 K and 67 K) and the superconducting state (67 K) spectra of σ_1 calculated using a version of the *hybrid approach* [55, 81], that is described in the following paragraph.

The hybrid approach uses an approximate expression for the Nambu Green's function, involving the dispersion relation of charged quasiparticles $\epsilon(\mathbf{k})$, the superconducting gap $\Delta_{\mathbf{k}}$, and a selfenergy correction $\hat{\Sigma} = \Sigma^{(0)} \hat{\tau}_0 + \Sigma^{(3)} \hat{\tau}_3 + \Sigma^{(1)} \hat{\tau}_1$:

$$\hat{G}(\omega, \mathbf{k}) = \frac{\tilde{\omega} \hat{\tau}_0 + \tilde{\epsilon}(\mathbf{k}) \hat{\tau}_3 + \tilde{\Delta}_{\mathbf{k}} \hat{\tau}_1}{\tilde{\omega}^2 - \tilde{\epsilon}^2(\mathbf{k}) - \tilde{\Delta}_{\mathbf{k}}^2}, \tag{12}$$

where $\tilde{\omega} = \omega - \Sigma^{(0)}(\omega, \mathbf{k})$, $\tilde{\epsilon}(\mathbf{k}) = \epsilon(\mathbf{k}) - \mu + \Sigma^{(3)}(\omega, \mathbf{k})$, $\tilde{\Delta}_{\mathbf{k}} = \Delta_{\mathbf{k}} + \Sigma^{(1)}(\omega, \mathbf{k})$. In contrast to [55, 81] (see also [49] and references therein), where $\hat{\Sigma}$ was obtained using a perturbative nonselfconsistent treatment of the coupling to spin fluctuations, we employ here the selfenergy resulting from our EAT based fits of the Y-123 data of [36]. The superconducting gap is approximated by the common d-wave ansatz

$$\Delta_{\mathbf{k}} = \frac{\Delta_{\max}}{2}\Big[\cos\big(k_x a\big) - \cos\big(k_y a\big)\Big] \tag{13}$$

and the components of $\hat{\Sigma}$ by

$$\Sigma^{(0)}(\omega, \mathbf{k}) = \Sigma_{AD}(\omega), \quad \Sigma^{(3)} = 0, \quad \Sigma^{(1)}(\omega, \mathbf{k}) = -\frac{\Sigma'_{AD}(\omega)}{\omega}\Delta_{\mathbf{k}}, \tag{14}$$

where Σ_{AD} is given by equations (10), (11), with $\alpha^2 F(\omega)$ from our fits of the 100 K and 67 K data and with the value of the gap depth of $h = 1$ (for the spectra of $\alpha^2 F$, see figure B1(d), h is defined by equation (B.2)). The construction of $\Sigma^{(1)}$ ensures that the gap of $A(\nu, \mathbf{k})$ is exactly equal to $\Delta_{\mathbf{k}}$ for $\epsilon(\mathbf{k}) = \mu$. The in-plane conductivity $\sigma(\omega)$ has been calculated using equations presented in subsection 3.1. The value of the plasma frequency $\omega_{\mathrm{pl,sc}}$, however, has not been obtained by a direct computation of the expression on the right hand side of equation (6), but using the sum rule

$$\omega_{\mathrm{pl,sc}}^2 = \omega_{\mathrm{pl}}^2 - \frac{2}{\pi\epsilon_0}\int_{0_+}^{\infty} \mathrm{d}\omega\sigma_1(\omega). \tag{15}$$

Here ω_{pl} is the (total) plasma frequency, that has been approximated by

$$\omega_{\mathrm{pl}}^2 = \frac{2}{\pi\epsilon_0}\int_0^{\infty} \mathrm{d}\omega\sigma_1^{\mathrm{n}}(\omega), \tag{16}$$

where $\sigma^{\mathrm{n}}(\omega)$ is the calculated normal state conductivity. We use the $t - t'$ dispersion relation with $t = 250$ meV and $t' = -100$ meV, $\mu = -350$ meV, and the values of N_p and d corresponding to Hg-1201.

The approach allows us to identify in a simple way the impact of the opening of the superconducting gap on the spectral structures. For the superconducting (normal) state we set $\Delta_{\max} = 40$ meV (0 meV). The normal state, 67 K, conductivity spectrum is very close (when multiplied by the conversion factor $2d_{\mathrm{Hg-1201}}/d_{\mathrm{Y-123}}$) to the experimental data of Y-123 and exhibits a dip with the HEOD around 125 meV. In the superconducting state, the feature is clearly shifted to higher energies, and the same applies to the spectra of M_1 and M_2 shown in figures 1(h) and 1(i). This is, however, in contradiction with the experimental data, where there is no comparable shift. The relatively small magnitude of the shift in the calculated spectra as compared to $\Delta_{\max}$ is a consequence of the Brillouin zone averaging with a major contribution of the near nodal quasiparticles. Note that a similar shift between the above and below T_c spectra, not occuring in the data, appears also in results of models, where the dip is solely due to an electron–boson coupling and the temperature dependence of the Fermi and Bose factors, for an example, see figure C1 of appendix C.

3.3. Optical conductivity calculated starting from the properties of the quasiparticle spectral function obtained by Reber and coworkers

Reber *et al* [10, 11] have recently analyzed their photoemission data of OPD and UD Bi-2212 using the *tomographic density of states*. This has led them to the observation that the near-nodal gap evolves smoothly through T_c and closes only at a temperature T_{close}, that is for UD samples considerably higher than T_c (see [11]) and presumably corresponds to T^{ons}. This is a photoemission data based indication of the precursor superconducting pairing scenario. Here we demonstrate that the energy scales of the infrared data and those of the photoemission ones are consistent with each other. We further argue that the data, taken together, suggest the presence of superconducting pairing correlations in the T-range from T_c to T^{ons}.

Figure 4 shows the spectra of σ_1 calculated using the type of parametrization of the quasiparticle spectral function, that has been used to fit the photoemission data in [10]: $A(\omega, \mathbf{k}) = -2\,\mathrm{Im}[G^{(0)}(\omega, \mathbf{k}) + G^{(3)}(\omega, \mathbf{k})]$, with $\hat{G}$ given by equation (12), $\Delta_{\mathbf{k}}$ by equation (13), $\hat{\Sigma}$ by equation (14), Σ''_{AD} by

$$\Sigma''_{AD}(\omega, T) = -\begin{cases} \Gamma(T) & \text{for} \quad |\omega| < \Omega_{\Gamma}, \\ \Gamma_{\infty} & \text{for} \quad \Omega_{\Gamma} \leqslant |\omega|, \end{cases} \tag{17}$$

and Σ'_{AD} by equation (11). The temperature dependence of $\Gamma(T)$ has been determined by the condition that $\Gamma(T)/\{1 - \lim_{\omega \to 0}[\Sigma'_{AD}(\omega)/\omega]\}$ equals the experimental value of the broadening parameter reported in figure 4 (a) of [10], corresponding to the UD Bi-2212 sample with $T_c = 67$ K. The values of the other input parameters are $\Omega_{\Gamma} = 70$ meV and $\Gamma_{\infty} = 150$ meV and $\Delta_{\max} = 40$ meV, with no temperature dependence for simplicity. The last one is consistent with figure 4(a) of [10]. We have used the same dispersion relation as in section 3.2 and the values of N_p and d corresponding to Y-123. The thin lines represent the spectra computed using the standard normal state formula, equation (8), not assuming any specific order. The thick lines have been obtained using the standard superconducting state formula, equation (7), with $A^{(1)}$ corresponding to the Nambu Green's function $\hat{G}$ introduced above. In both cases the sum over $\mathbf{k}$ entering the expression for σ_1 runs over the restricted region of the Brillouin zone that is shaded in the inset of figure 4 , i.e., over the region addressed in [10].It is clear from the data of [10], that this region is not significantly influenced by the antinodal pseudogap setting on at $T^{\star}$.
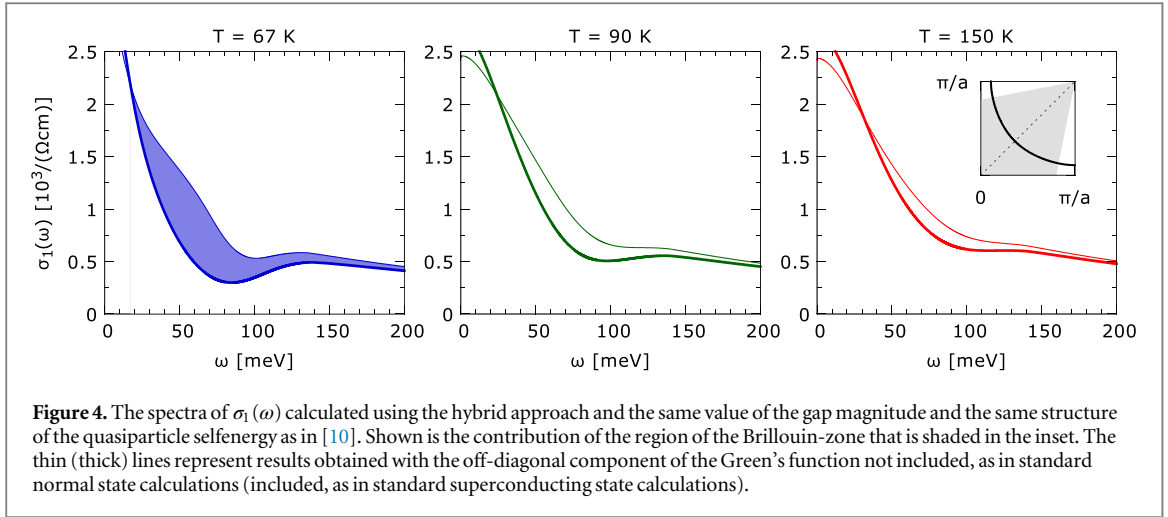
Figure 4. The spectra of $\sigma_1(\omega)$ calculated using the hybrid approach and the same value of the gap magnitude and the same structure of the quasiparticle selfenergy as in [10]. Shown is the contribution of the region of the Brillouin-zone that is shaded in the inset. The thin (thick) lines represent results obtained with the off-diagonal component of the Green's function not included, as in standard normal state calculations (included, as in standard superconducting state calculations).
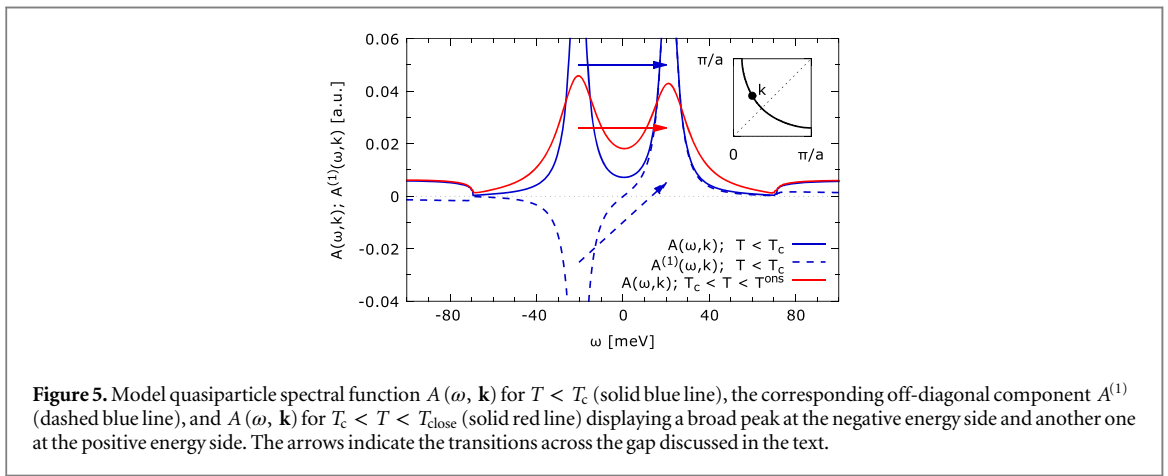
Figure 5. Model quasiparticle spectral function $A(\omega, \mathbf{k})$ for $T < T_c$ (solid blue line), the corresponding off-diagonal component $A^{(1)}$ (dashed blue line), and $A(\omega, \mathbf{k})$ for $T_c < T < T_{close}$ (solid red line) displaying a broad peak at the negative energy side and another one at the positive energy side. The arrows indicate the transitions across the gap discussed in the text.

Note that the thin (artificial normal state) lines are shown merely to illustrate the role of the off-diagonal component of $\hat{A}$ determining the coherence factor.

First of all, it can be seen that the HEOD occurs at an energy very close to that of the experimental infrared data of UD cuprates. Second, from the two blue lines, only the thick one is qualitatively consistent with the data for temperatures slightly above T_c. The thin one displays a pronounced shoulder feature in the middle of the dip, that the experimental data do not contain. The energy of the structure is determined by Δ_{max}, here it is located at ca 60 meV. The feature persists to some extent to higher temperatures—note the differences between the onsets at the high energy side of the low energy maximum of σ_1 in the thick lines and those in the thin lines. It corresponds to 'transitions across the gap'. What we mean is the following: the expression on the right hand side of equation (8) (see the factor $A(\nu, \mathbf{k}) A(\nu + \omega, \mathbf{k}) [f(\nu) - f(\nu + \omega)]$) can be thought of as a sum of contributions of different 'transitions' between ν and $\nu + \omega$, for $T \to 0$ between occupied states at negative energies and unoccupied states at positive energies. A pronounced contribution can be expected to originate from transitions between the broad peaks at the negative energy side and those at the positive energy side—the transitions across the gap. For a schematic representation of the transitions, see figure 5. In the superconducting state below T_c, the contribution to $\sigma_1(\omega)$ of the transitions across the gap denoted in figure 5 by the solid blue arrow ($A \to A$) is compensated by the contribution of the transitions denoted by the dashed blue arrow ($A^{(1)} \to A^{(1)}$, see the second term in the integral of equation (7)). This is a manifestation of the characteristic coherence factor [82] described here by $A^{(1)}$. In the spectra calculated using the unrealistic normal state model for $T_c < T < T^{ons}$, the contribution of the transitions across the gap denoted by the solid red arrow in figure 5, is not compensated and yields the structure in the middle of the dip in figure 4.

The absence of the structure in the above T_c experimental data indicates the persistence of the coherence factor of superconducting pairing correlations above T_c. In fact, we are not aware of any ordered state not involving superconducting pairing that would be consistent with Reber's observations and at the same time exhibit a coherence factor consistent with the infrared data. For simple charge and spin density wave systems, the relevant coherence factor is such that the contribution of the transitions across the gap is enhanced rather than

fully suppressed. For a discussion of the coherence factors of density waves, see [82], for examples of conductivity spectra of density wave compounds displaying the 2Δ peak due to the transitions, see [83–85]. A clear 2Δ peak appears also in the calculated spectra corresponding to the *d*-density-wave model [86]. Fujita and coworkers reported recently a complex pattern of the charge distribution associated with the density wave occurring in UD cuprates [87]. To the best of our knowledge, possible consequences for the coherence factors have not been investigated thus far.

Finally, we would like to comment on the fate of the spectral weight of the transitions across the gap indicated in figure 5. In the true superconducting state the loss of this spectral weight caused by the presence of $A^{(1)}$ is compensated by the formation of the δ-peak at $\omega = 0$. In the normal state, for $T_c < T < T^{ons}$, there is no long range phase coherence and therefore $A^{(1)} = 0$. The persisting pairing correlations, however, must provide a vertex correction to the right hand side of equation (8) playing a similar role as $A^{(1)}$ below T_c, i.e., a correction partially reducing the spectral weight of the transitions across the gap. The lost spectral weight can be expected to reappear at low energies, in the contribution to σ_1 of collective degrees of freedom associated with the pairing correlations.

4. Summary and Conclusions

The published experimental data of $\sigma_1(\omega)$ of UD high-T_c cuprate superconductors (HTCS) display a clear dip feature below ca 130 meV, that starts to develop at $T^{ons} > T_c$. This dip feature gives rise to corresponding structures of the memory function. The features are similar to those of OPD HTCS, where they set in very close to T_c and are commonly assigned to superconductivity and well understood in terms of the Eliashberg theory. This similarity and the one between the data and our calculated (Eliashberg) spectra strongly suggest that the dip feature of the UD HTCS is also due to superconducting pairing correlations and its persistence in the temperature range from T_c to T^{ons} due to the presence of a precursor superconducting pairing phase. In order to support this interpretation, we have further demonstrated that (a) the temperature dependence of the dip feature cannot be simply accounted for in terms of a normal state gap unrelated to superconductivity, or in terms of normal fermions coupled to bosons, and (b) that the infrared data taken together with findings of recent photoemission studies employing the tomographic density of states indicate the persistence of the coherence factor characteristic of superconducting pairing correlations in a range of temperatures above T_c. Future studies should focus on clarifying the relation between the superconducting pairing correlations and the observed charge density waves and on the origin of the Fermi-liquid like scaling of $M(\omega)$ in the temperature range from T_c to T^{ons}.

Acknowledgments

Appendix A. Generalized Eliashberg equations: detailed account of the computational approach and the values of input parameters

Within the framework of the spin-fermion model used to obtain the data presented in figures 1(d)–(f), the superconductivity emerges in a similar way as in a coupled electron–phonon system of a conventional superconductor. The retarded pairing interaction is mediated by spin fluctuations replacing the phonons of the conventional case and coupling to the spin of the quasiparticles instead of their charge, for reviews, see [46–51]. A quantitative treatment of the spin-fermion model can be based on the generalized Eliashberg equations, see, e.g., [58]. The matrix selfenergy $\hat{\Sigma}$, in terms of Pauli matrices $\hat{\Sigma} = \Sigma^{(0)}\hat{\tau}_0 + \Sigma^{(3)}\hat{\tau}_3 + \Sigma^{(1)}\hat{\tau}_1$, is determined by the selfconsistent equation

$$\hat{\Sigma}\left(i\omega_n, \mathbf{k}\right) = \frac{g^2}{\beta N}\sum_{m,\mathbf{q}}\chi\left(i\nu_m, \mathbf{q}\right)\hat{G}\left(i\omega_n - i\nu_m, \mathbf{k} - \mathbf{q}\right),$$ (A.1)

involving the renormalized quasiparticle propagator

$$\hat{G}^{-1}\left(i\omega_n, \mathbf{k}\right) = i\omega_n\hat{\tau}_0 - [\epsilon(\mathbf{k}) - \mu]\hat{\tau}_3 - \hat{\Sigma}\left(i\omega_n, \mathbf{k}\right),$$ (A.2)

and the spin susceptibility $\chi(i\nu_m, \mathbf{q})$, where $i\omega_n$ are the Matsubara energies for fermions and $i\nu_m$ for bosons. The value of the coupling constant g can be adjusted so that realistic values of the superconducting gap and of the transition temperature are obtained.

A direct solution of equation (A.1) in Matsubara energies has to be followed by a numerical analytical continuation of the selfenergy to the real axis which is an ill-posed problem. To avoid the numerical difficulties, one can employ the spectral representation of the quasiparticle propagator

$$\hat{G}\left(i\omega_n, \mathbf{k}\right) = \int_{-\infty}^{\infty}\frac{d\omega}{2\pi}\frac{\hat{A}(\omega, \mathbf{k})}{i\omega_n - \omega},$$ (A.3)

where $\hat{A} = A^{(0)}\hat{\tau}_0 + A^{(3)}\hat{\tau}_3 + A^{(1)}\hat{\tau}_1$ is defined by $\hat{A}(\omega, \mathbf{k}) = -2\,\mathrm{Im}\{\hat{G}(\omega + i0, \mathbf{k})\}$ and also of the spin susceptibility

$$\chi\left(i\nu_m, \mathbf{q}\right) = -\frac{1}{\pi}\int_{-\infty}^{\infty}\frac{\chi''(\nu, \mathbf{q})}{i\nu_m - \nu}d\nu.$$ (A.4)

By inserting the spectral representations in equation (A.1), the following expression for the imaginary part of the retarded selfenergy on the real axis can be obtained

$$\hat{\Sigma}''(\omega, \mathbf{k}) = \frac{g^2}{N}\sum_{\mathbf{q}}\int_{-\infty}^{\infty}\frac{d\nu}{2\pi}\chi''(\nu, \mathbf{q})\hat{A}(\omega - \nu, \mathbf{k} - \mathbf{q})[f(\omega - \nu) - b(\nu) - 1],$$ (A.5)

where $f(\omega)$ and $b(\nu)$ are the Fermi and the Bose functions, respectively. The corresponding real part of the selfenergy is calculated via the Kramers–Kronig transformation. The evaluation of the expression on the right hand side of equation (A.5) represents the most demanding part of the calculation due to the $\mathbf{q}$, ν-summation for every $(\omega, \mathbf{k})$. The computational effort can be greatly reduced by using the fact that the expression can be written as a difference of two convolutions of the form

$$X \star Y\,|_{\omega,\mathbf{k}} = \frac{1}{N}\sum_{\mathbf{q}}\int_{-\infty}^{\infty}X(\nu, \mathbf{q})Y(\omega - \nu, \mathbf{k} - \mathbf{q})d\nu,$$ (A.6)

which can be efficiently evaluated using the fast Fourier transform algorithm. With the above definition, a compact expression for Σ'' reads

$$\Sigma''^{(\alpha)} = g^2\left[\chi'' \star \left(f - \frac{1}{2}\right)A^{(\alpha)} - \left(b + \frac{1}{2}\right)\chi'' \star A^{(\alpha)}\right], \qquad \alpha = 0, 3, 1.$$ (A.7)

We have solved the selfconsistent equations for the selfenergy iteratively starting with a BCS spectral function. The bare quasiparticles were described by the tight-binding dispersion

$$\epsilon(\mathbf{k}) = -2t\left[\cos\left(k_x a\right) + \cos\left(k_y a\right)\right] - 4t'\cos\left(k_x a\right)\cos\left(k_y a\right),$$ (A.8)

with $t = 380$ meV and $t' = -120$ meV, $a = 3.828$ Å. The same form of the model spin susceptibility containing the resonance mode and a continuum as in [55, 56] was employed,

$$\chi_{SF}(\omega, \mathbf{q}) = b_{RM}\chi_{RM}(\omega, \mathbf{q}) + b_C\chi_C(\omega, \mathbf{q}),$$

$$\chi_{RM}(\omega, \mathbf{q}) = \frac{1}{1 + (\mathbf{q} - \mathbf{Q})^2\xi^2}\frac{F_{RM}}{\omega_0^2 - \omega^2 - i\Gamma\omega},$$

$$\chi_C(\omega, \mathbf{q}) = \frac{1}{1 + (\mathbf{q} - \mathbf{Q})^2\xi_C^2}\frac{F_C}{\omega_C^2 - \omega^2 - i\Gamma_C\omega},$$

where $\mathbf{Q} = (\pi/a, \pi/a)$ and the values of F_{RM} and F_C are determined by a normalization condition presented in [55]. Here we have set $\hbar\omega_0 = 50$ meV, $\Gamma = 20$ meV, $\xi = 2.5a$, $\hbar\omega_C = 400$ meV, $\Gamma_C = 1000$ meV, $\xi_C = 1.5a$, $b_M = 2$, and $b_C = 4$. The main differences with respect to the input values of [56] are: the energy of the resonance $\hbar\omega_0$ is slightly higher (40 meV in [56]), the 'coherence length' ξ_C of the continuum is ca three times higher, and the dimensionless spectral weight of the resonance b_M is twice as high. With these values of the parameters, the value of the coupling constant of $g = 3$ eV leads to $T_c = 133$ K and $\Delta_{max} = 45$ meV.

After every iteration, the chemical potential μ was adjusted to keep the electron occupancy at $n_{el} = 0.85$. Working with the spectral functions, n_{el} is evaluated by using the formula
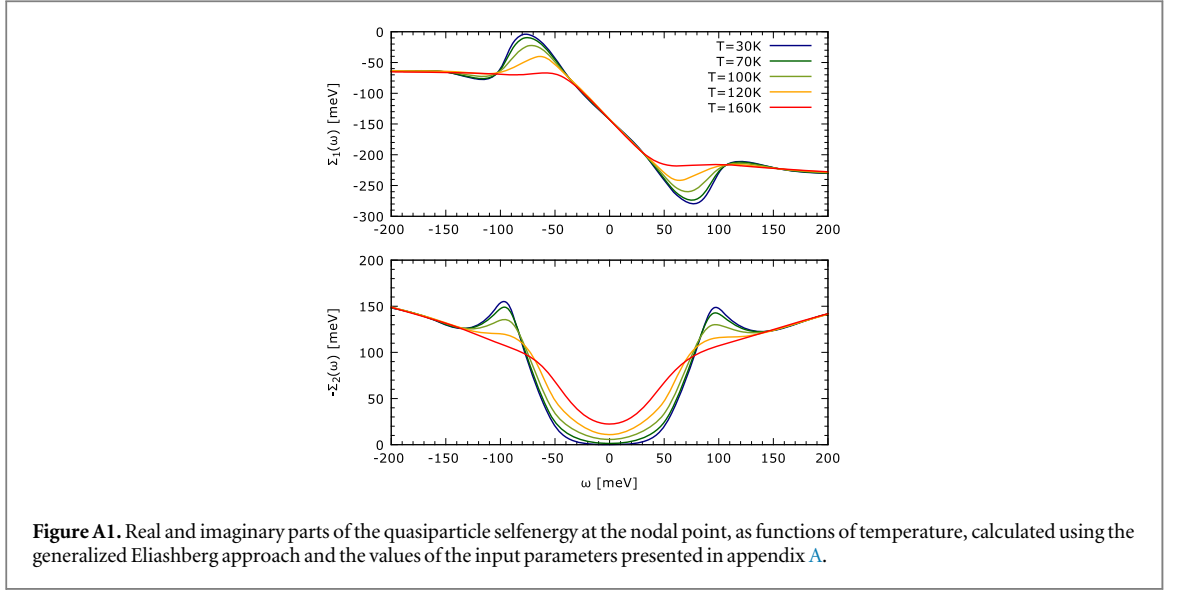
Figure A1. Real and imaginary parts of the quasiparticle selfenergy at the nodal point, as functions of temperature, calculated using the generalized Eliashberg approach and the values of the input parameters presented in appendix A.

$$n_{\mathrm{el}} = 1 - \frac{1}{N} \sum_{\mathbf{k}} \int_{-\infty}^{\infty} \frac{\mathrm{d}E}{2\pi} A^{(3)}(E, \mathbf{k}) \tanh \frac{\beta E}{2}. \tag{A.9}$$

For the sampling of the selfenergy, we have used a grid of 128×128 points in the Brillouin zone and the energy axis was discretized using 32768 points covering uniformly the energy range $(-4 \ \mathrm{eV}, +4 \ \mathrm{eV})$.

Figure A1 shows examples of our intermediate results: the real and imaginary parts of the quasiparticle selfenergy at the nodal point as functions of temperature.

Appendix B. EAT with a gap in the density of states

The aim of this section is to explore to what extent we can reproduce the experimental data of the in-plane conductivity in the temperature range $T_{\mathrm{c}} < T < T^{\star}$ using the EAT. A special attention is paid to the experimental trend occurring below T^{ons}. Our starting point is the fitting procedure developed by Hwang, Sharapov and Carbotte [37, 39]. This formalism has been slightly modified so that it is somewhat more rigorous, involves less fitting parameters and also allows one to evaluate all important optical functions.

To describe the model we begin with the boson spectral function $\alpha^2 F$. The Ansatz consists of a single peak described by two parameters A_{s} and ω_{s}

$$\alpha^2 F(\omega) = \frac{A_{\mathrm{s}} \omega}{\omega^4 + \omega_{\mathrm{s}}^4}, \quad 0 < \omega < \omega_{\mathrm{c}}, \tag{B.1}$$

an example is shown in figure B3(c). The density of states $N(\omega)$ occurring in the formula for the selfenergy reads

$$N(\omega) = \begin{cases} 1 - h\left(1 - \left(\dfrac{\omega}{\Delta_{\mathrm{pg}}}\right)^2\right) & \text{for} \quad \omega < \Delta_{\mathrm{pg}}, \\[2mm] 1 + \dfrac{2}{3}h & \text{for} \quad \Delta_{\mathrm{pg}} < \omega < 2\Delta_{\mathrm{pg}}, \\[2mm] 1 & \text{for} \quad 2\Delta_{\mathrm{pg}} < \omega, \end{cases} \tag{B.2}$$

for an example, see figure B3(d). Fixing the width of the pseudogap at $\Delta_{\mathrm{pg}} = 35$ meV, the end of the 'recovery region' [38] at $2\Delta_{\mathrm{pg}}$ and conserving the number of states, we have only 2+1 fitting parameters in total—A_{s}, ω_{s} and the pseudogap depth h. The selfenergy Σ is calculated within the non–selfconsistent Fock approximation with the gapped density of states N. For the imaginary part of the retarded selfenergy we have [37]

$$\Sigma_2(\omega) = -\pi \int_0^{\infty} \mathrm{d}\nu \, \alpha^2 F(\nu) \{ N(\omega - \nu)[b(\nu) + 1 - f(\omega - \nu)] + N(\omega + \nu)[b(\nu) + f(\omega + \nu)] \}. \tag{B.3}$$

Figure B1. (a), (b) Results of the fitting procedure described in the text applied to the experimental data of underdoped Y-123 reported in [36]. The data (gray lines) are presented for selected temperatures only. We can see that the quality of the fit is good for all temperatures studied. (c) The resulting spectra of σ_1 together with selected data. (d) The obtained temperature dependence of the function $\alpha^2 F$. We see that with decreasing temperature the maximum of $\alpha^2 F$ grows and shifts to lower frequencies. The inset shows the temperature dependence of the gap volume $2/3 h\Delta_{pg}$. At 295 K the best fit is with no gap in the density of states and thus the gap volume is zero. Below this temperature the gap volume shows a weak temperature dependence, but with a significant variance.

The real part Σ_1 is obtained using the Kramers–Kronig relation

$$\Sigma_1(\omega) = -\frac{1}{\pi} \mathcal{P} \int_{-\infty}^{\infty} d\nu \frac{\Sigma_2(\nu)}{\omega - \nu}. \tag{B.4}$$

The conductivity is calculated using the Allen's theory [77, 78]

$$\chi(\omega) = \int_{-\infty}^{\infty} d\epsilon \frac{f(\epsilon) - f(\omega + \epsilon)}{\omega - \Sigma(\omega + \epsilon) + \Sigma^{\star}(\omega)}, \tag{B.5}$$

$$\sigma(\omega) = \frac{i\epsilon_0}{\hbar} \frac{\omega_p^2}{\omega} \chi(\omega), \tag{B.6}$$

where ω and ω_{pl} are in units of energy. For the sake of simplicity the integration in (B.5) does not involve the non–constant density of states N. The memory function M is obtained as
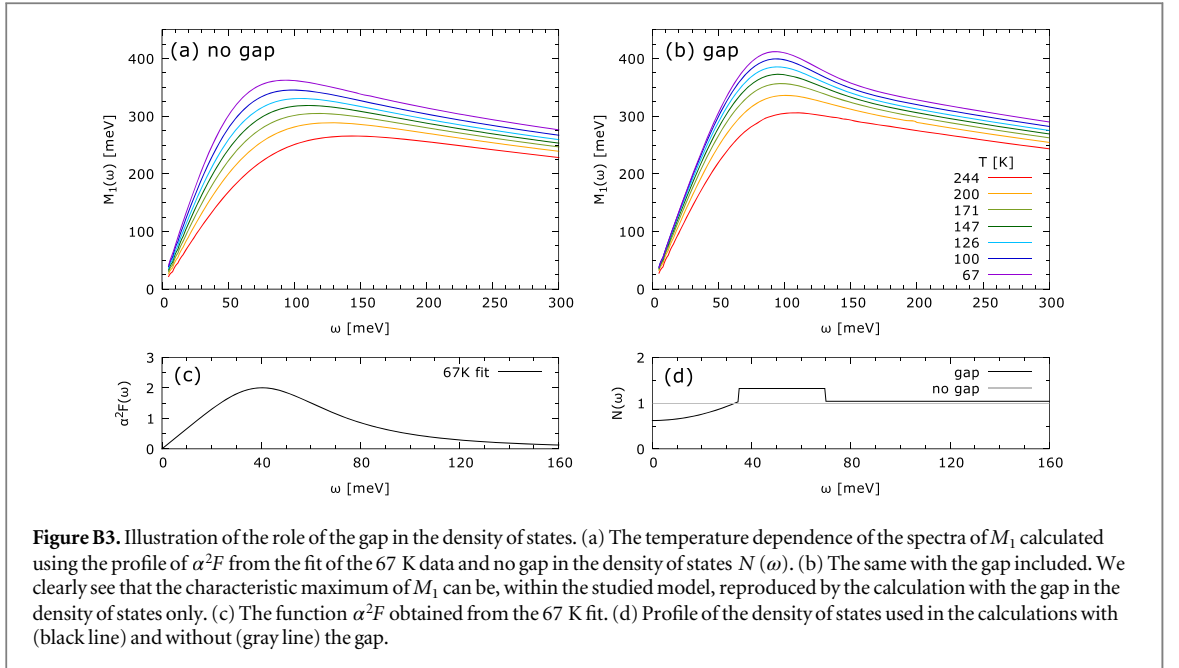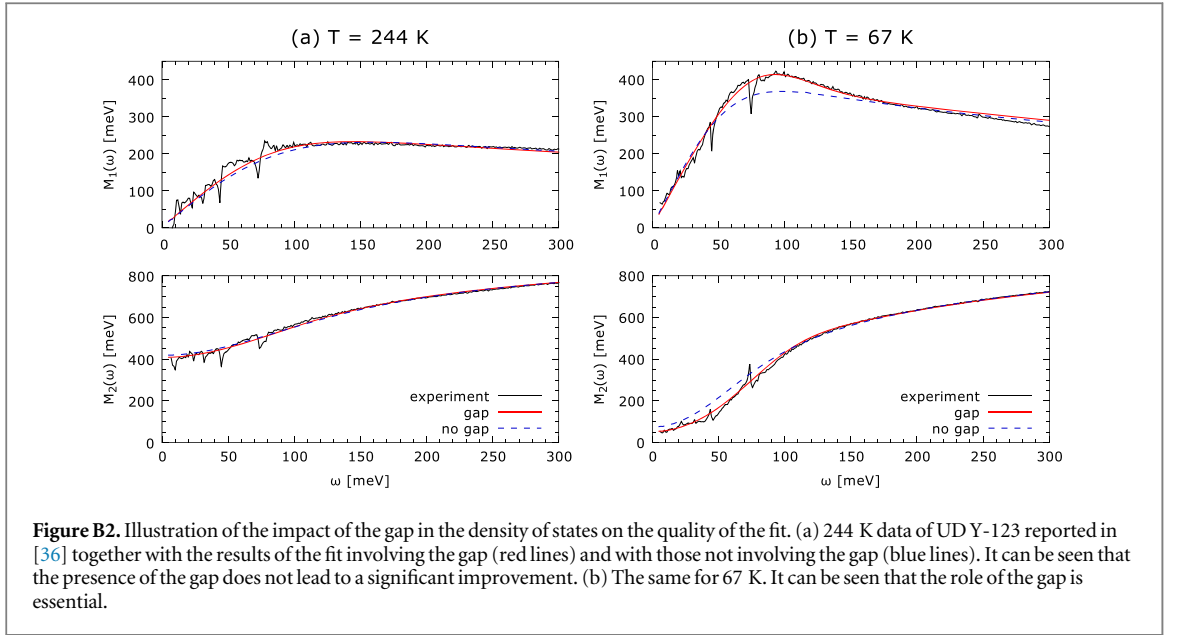
$$M(\omega) = -\omega \left\{ \frac{1}{\chi(\omega)} + 1 \right\}. \tag{B.7}$$

Here is the main formal difference between our approach and the one by Hwang *et al* [39], where a simplified expression, obtained by a series expansion of the right hand side of equation (B.5) in powers of the selfenergy is used to calculate M_2.

The values of the parameters A_s, ω_s and h have been obtained by minimizing $\int_{30\,\text{meV}}^{400\,\text{meV}} |M_{\text{num}}(\nu) - M_{\text{exp}}(\nu)| d\nu$ using simulated annealing followed by a simplex method. Here M_{num} is a result of the calculations described above and M_{exp} is derived from experimental data.

We have applied the described fitting procedure to the experimental data of ε_1 and σ_1 obtained by Hwang *et al* [36]. To obtain M_{exp} from the data we have set $\epsilon_\infty = 3.6$. We have further set $\hbar\omega_{pl} = 2350$ meV (temperature independent), so that $m^{\star}(\omega)/m = M_1(\omega)/\omega + 1 \approx 1$ at $\omega = 1$ eV (as in [88]). Results of the fitting procedure are shown in figure B1. The experimental data (gray lines) are presented for several temperatures only. We can see that the quality of the fits is good in the whole range of temperatures. For each temperature we run the procedure several times. The final $\alpha^2 F$ is usually almost identical. The maximum of $\alpha^2 F$ grows monotonically and shifts to lower frequencies with decreasing temperature, see figure B1 (d). The gap volume $\frac{2}{3} h\Delta_{pg}$, shown in the inset of (d), is equal to zero at 295 K and at lower temperatures displays a weak temperature dependence but with a significant variance of its value.

Closer look at the results for lower and higher temperatures reveals a clear difference in the role of the gap. In figure B2 we compare results obtained by the above described 2+1 parameter model with those obtained using the 2 parameter model with no gap in the density of states. In (a) we see that for higher temperatures the gap does not play any essential role. It only helps to improve the fit quality slightly. On the other hand in (b) we see that for

Figure B2. Illustration of the impact of the gap in the density of states on the quality of the fit. (a) 244 K data of UD Y-123 reported in [36] together with the results of the fit involving the gap (red lines) and with those not involving the gap (blue lines). It can be seen that the presence of the gap does not lead to a significant improvement. (b) The same for 67 K. It can be seen that the role of the gap is essential.

Figure B3. Illustration of the role of the gap in the density of states. (a) The temperature dependence of the spectra of M_1 calculated using the profile of α^2F from the fit of the 67 K data and no gap in the density of states $N(\omega)$. (b) The same with the gap included. We clearly see that the characteristic maximum of M_1 can be, within the studied model, reproduced by the calculation with the gap in the density of states only. (c) The function α^2F obtained from the 67 K fit. (d) Profile of the density of states used in the calculations with (black line) and without (gray line) the gap.

lower temperatures the features in M_1 and M_2, which are discussed in the main text, can be well reproduced only by the model including the gap in the density of states. This is shown in more detail in figure B3 , where we present the spectra of M_1 calculated using the α^2F from the fit of the 67 K data (a) without and (b) with the gap in the density of states included. The results confirm that within the studied model the discussed low-temperature feature of M_1 is due to the gap in N.

In figure B4 we review some important characteristics of both types of fits—with and without the gap in N. The measure of the quality of the fit in (a) is given by the integral norm $|M_{\mathrm{num}} - M_{\mathrm{exp}}|$ described above. We see that for higher temperatures both fits are of a comparable quality. For temperatures closer to T_c, starting from ca 200 K, better results are achieved by the approach with a nonzero gap in N. In (b) we show the temperature dependence of the integrated spectral weight, $\mathrm{SW}(\omega_1, \omega_2) = \int_{\omega_1}^{\omega_2} \mathrm{d}\nu\sigma_1(\nu)$ of the experimental data from [36].

Comparison of (a) and (b) reveals that the temperature, below which the gap in N is necessary for achieving a good quality of the fit, approximately coincides with the temperature of the onset of the spectral weight shift from the frequency range 30–200 meV to lower frequencies, see the green and the yellow lines in figure B4(b). This temperature scale was recognized already in [6] and found to be close to T^{ons} of the c-axis data. The temperature dependence of the frequency ω_{max} of the maximum of the boson spectral density in (c) and that of
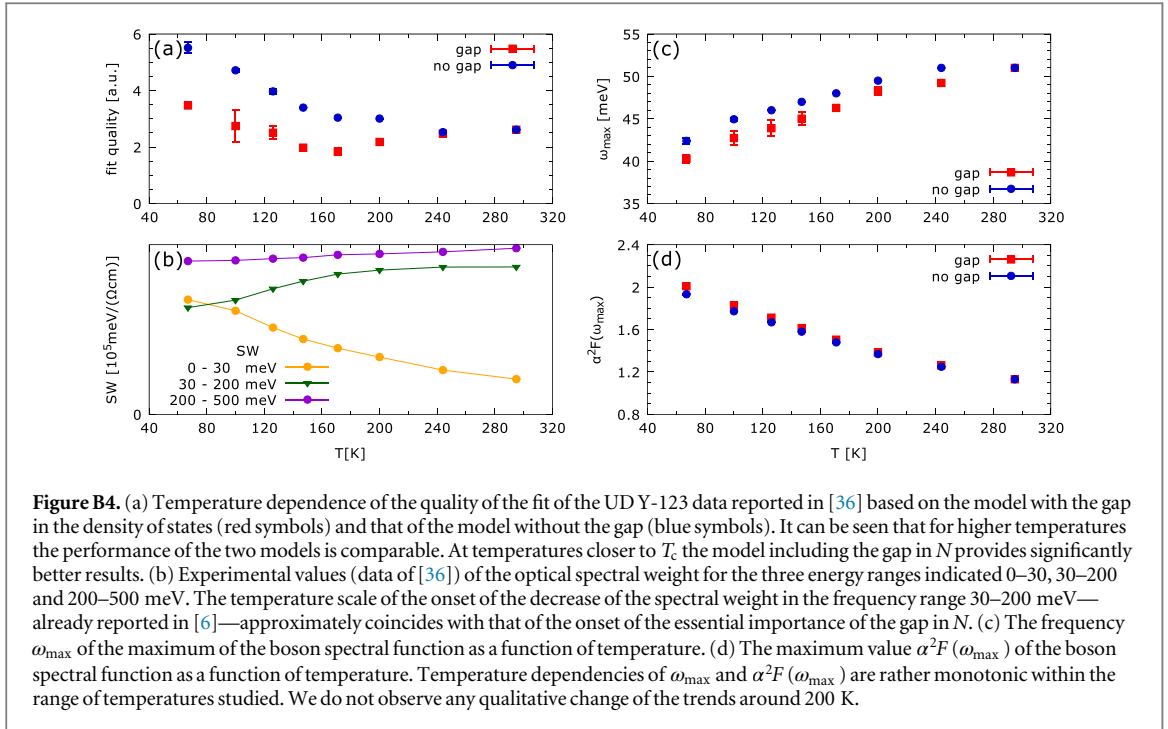
Figure B4. (a) Temperature dependence of the quality of the fit of the UD Y-123 data reported in [36] based on the model with the gap in the density of states (red symbols) and that of the model without the gap (blue symbols). It can be seen that for higher temperatures the performance of the two models is comparable. At temperatures closer to T_c the model including the gap in N provides significantly better results. (b) Experimental values (data of [36]) of the optical spectral weight for the three energy ranges indicated 0–30, 30–200 and 200–500 meV. The temperature scale of the onset of the decrease of the spectral weight in the frequency range 30–200 meV— already reported in [6]—approximately coincides with that of the onset of the essential importance of the gap in N. (c) The frequency ω_{max} of the maximum of the boson spectral function as a function of temperature. (d) The maximum value $\alpha^2 F(\omega_{max})$ of the boson spectral function as a function of temperature. Temperature dependencies of ω_{max} and $\alpha^2 F(\omega_{max})$ are rather monotonic within the range of temperatures studied. We do not observe any qualitative change of the trends around 200 K.
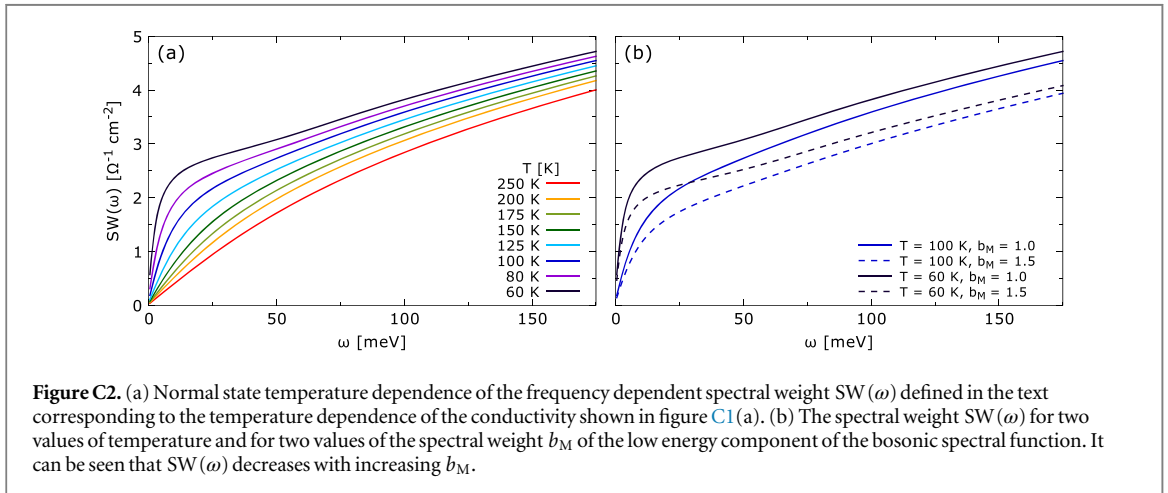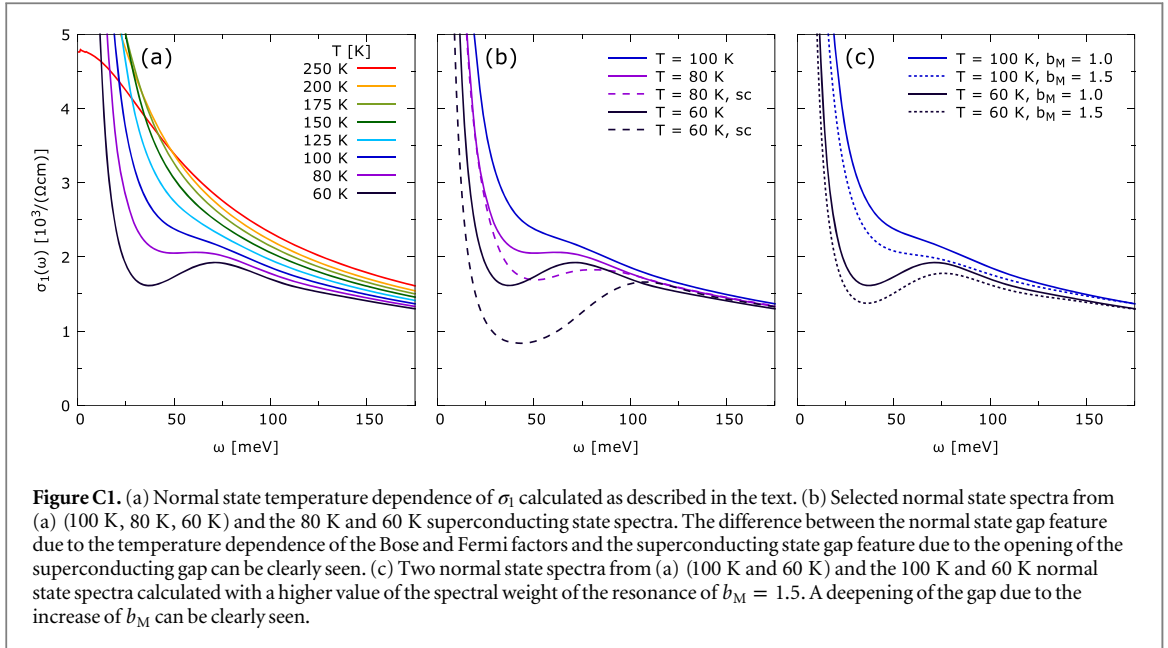
$\alpha^2 F(\omega_{max})$ in (d) are rather monotonic for both methods. There is no apparent change of the basic trend within the range of temperatures studied.

In summary, we have fitted the experimental data reported by Hwang *et al* [36] by the model with and without the gap in the density of states. Comparison of the results shows that at high temperatures the model which uses the boson spectral function $\alpha^2 F$ and an energy independent density of states is sufficient for a reasonable description of the data. On the other hand, for temperatures closer to T_c, the gap in N becomes crucial for reproducing the specific features of M_1 and M_2. The fitting procedure reveals the presence of a characteristic temperature located around 200 K, below which the presence of the gap in the density of states is necessary. This temperature scale is obviously connected to that described in [6] (see the corresponding supporting material).

Appendix C. Remarks on purely normal-state interpretations of the dip feature

First, a dip in the in-plane conductivity develops with decreasing temperature naturally, even in the absence of a DOS gap, due to the temperature dependence of the Bose and Fermi factors. Its scale is determined by the characteristic boson energy and it is typically narrower than in the data. An example of a standard normal state temperature dependence of σ_1 is shown in figure C1(a). The spectra have been calculated using the Eliashberg formalism described in appendix A and the same values of the input parameters as in [56], except for $t = 0.38$ eV, $t' = -0.120$ eV, $n = 0.85$ and $g = 3.0$ eV, for definitions, see [56] and [55]. The onset of superconductivity leads to a different shape of the gap. This is illustrated in figure C1(b) showing the 100 K, 80 K and 60 K normal state spectra from (a), and the 80 K and 60 K superconducting state spectra. For the present values of the input parameters, $T_c = 90$ K.

Second, a deepening of the dip for a fixed temperature can be achieved by increasing the spectral weight of the low-energy component of the bosonic spectral function ($\alpha^2 F$ in the Allen's theory, $\chi''(\mathbf{q}, \omega)$ in more realistic models involving spin fluctuations). The latter increase, however, also leads to a reduction of the total optical spectral weight in the infrared, not occurring in the data. This problem is illustrated in figures C1(c) and C2. Figure C1(c) shows the 100 K and 60 K normal state spectra from (a) and the 100 K and 60 K normal state spectra calculated with a higher value of the dimensionless spectral weight of the resonance of $b_M = 1.5$ (the dimensionless spectral weight of the continuum b_C is reduced accordingly, from $b_C = 4.0$ to $b_C = 3.5$). The deepening of the minimum can be clearly seen. Figure C2(a) shows the calculated normal state temperature dependence of the spectral weight $SW(\omega) = \int_0^\omega \sigma_1(\omega') d\omega'$ corresponding to the spectra of figure C1(a), that is qualitatively consistent with the experimental one shown in figure 4 of [36]. With decreasing temperature, $SW(\omega)$ at low frequencies *increases*. Figure C2(b) shows that the increase of b_M, for a fixed temperature, leads to the opposite trend: with increasing b_M the spectral weight at low frequencies *decreases*. It is thus unlikely that the

Figure C1. (a) Normal state temperature dependence of σ_1 calculated as described in the text. (b) Selected normal state spectra from (a) (100 K, 80 K, 60 K) and the 80 K and 60 K superconducting state spectra. The difference between the normal state gap feature due to the temperature dependence of the Bose and Fermi factors and the superconducting state gap feature due to the opening of the superconducting gap can be clearly seen. (c) Two normal state spectra from (a) (100 K and 60 K) and the 100 K and 60 K normal state spectra calculated with a higher value of the spectral weight of the resonance of $b_M = 1.5$. A deepening of the gap due to the increase of b_M can be clearly seen.

Figure C2. (a) Normal state temperature dependence of the frequency dependent spectral weight SW(ω) defined in the text corresponding to the temperature dependence of the conductivity shown in figure C1(a). (b) The spectral weight SW(ω) for two values of temperature and for two values of the spectral weight b_M of the low energy component of the bosonic spectral function. It can be seen that SW(ω) decreases with increasing b_M.

formation of the gap in σ_1 could be described as being solely due to a specific temperature dependence of the low-energy component of $\alpha^2 F$ or $\chi''(\mathbf{q}, \omega)$.

References

[1] Wang Y, Li L and Ong N P 2006 *Phys. Rev. B* **73** 024510
[2] Li L, Wang Y, Komiya S, Ono S, Ando Y, Gu G D and Ong N P 2010 *Phys. Rev. B* **81** 054510
[3] Li L, Wang Y and Ong N P 2013 *Phys. Rev. B* **87** 056502
[4] Gomes K K, Pasupathy A N, Pushp A, Ono S, Ando Y and Yazdani A 2007 *Nature* **447** 569
[5] Lee J, Fujita K, Schmidt A R, Kim C K, Eisaki H, Uchida S and Davis J C 2009 *Science* **325** 1099
[6] Dubroka A *et al* 2011 *Phys. Rev. Lett.* **106** 047006
[7] Uykur E, Tanaka K, Masui T, Miyasaka S and Tajima S 2014 *Phys. Rev. Lett.* **112** 127003
[8] Kaiser S *et al* 2014 *Phys. Rev. B* **89** 184516
[9] Kondo T, Hamaya Y, Palczewski A D, Takeuchi T, Wen J S, Xu Z J, Gu G, Schmalian J and Kaminski A 2011 *Nat. Phys.* **7** 21
[10] Reber T J *et al* 2012 *Nat. Phys.* **8** 606
[11] Reber T J *et al* 2013 *Phys. Rev. B* **87** 060506(R)
[12] Zhang W, Smallwood C L, Jozwiak C, Miller T L, Yoshida Y, Eisaki H, Lee D H and Lanzara A 2013 *Phys. Rev. B* **88** 245132
[13] Tallon J L, Barber F, Storey J G and Loram J W 2013 *Phys. Rev. B* **87** 140508(R)
[14] Rullier-Albenque F, Alloul H and Rikken G 2011 *Phys. Rev. B* **84** 014522
[15] Mahyari Z L, Cannell A, de Mello E V L, Ishikado M, Eisaki H, Liang R, Bonn D and Sonier J 2013 *Phys. Rev. B* **88** 144504
[16] van der Marel D and Tsvetkov A 1996 *Czech J. Phys.* **46** 3165
[17] Grüninger M, van der Marel D, Tsvetkov A A and Erb A 2000 *Phys. Rev. Lett.* **84** 1575
[18] Munzar D, Bernhard C, Golnik A, Humlíček J and Cardona M 1999 *Solid State Commun.* **112** 365
[19] Železný V, Tajima S, Munzar D, Motohashi T, Shimoyama J and Kishio 2001 *Phys. Rev. B* **63** 060502
[20] Dubroka A and Munzar D 2004 *Physica* C **405** 133

[21] Shah N and Millis A J 2001 *Phys. Rev.* B **65** 024506
[22] Chaloupka J, Bernhard C and Munzar D 2009 *Phys. Rev.* B **79** 184513
[23] Vašátko J and Munzar D 2012 *Phys. Rev.* B **86** 014512
[24] Ghiringhelli G *et al* 2012 *Science* **337** 821
[25] Chang J *et al* 2012 *Nat. Phys.* **8** 871
[26] Walstedt R E, Warren W W, Bell R F, Cava R J, Espinosa G P, Schneemeyer L F and Waszczak J V 1990 *Phys. Rev.* B **41** 9574(R)
[27] Homes C C, Timusk T, Liang R, Bonn D A and Hardy W N 1993 *Phys. Rev. Lett.* **71** 1645
[28] For a review, see Timusk T and Statt B 1999 *Rep. Prog. Phys.* **62** 61
[29] For a review, see Timusk T 2003 *Solid State Commun.* **127** 337
[30] Yu L, Munzar D, Boris A V, Yordanov P, Chaloupka J, Wolf T, Lin C T, Keimer B and Bernhard C 2008 *Phys. Rev. Lett.* **100** 177004
[31] Krasnov V M, Yurgens A, Winkler D, Delsing P and Claeson T 2000 *Phys. Rev. Lett.* **84** 5860
[32] Krasnov V M 2015 arXiv:condmat/1501.03995
[33] For a review see Hashimoto M, Vishik I M, He R H, Devereaux T P and Shen Z X 2014 *Nat. Phys.* **10** 483
[34] Shekhter A, Ramshaw B J, Liang R, Hardy W N, Bonn D A, Balakirev F F, McDonald R D, Betts J B, Riggs S C and Migliori A 2013 *Nature* **498** 75
[35] Mirzaei S I *et al* 2013 *Proc. Natl Acad. Sci. USA* **110** 5774
[36] Hwang J, Yang J, Timusk T, Sharapov S G, Carbotte J P, Bonn D A, Liang R and Hardy W N 2006 *Phys. Rev.* B **73** 014508
[37] Sharapov S G and Carbotte J P 2005 *Phys. Rev.* B **72** 134506
[38] Hwang J, Carbotte J P and Timusk T 2008 *Phys. Rev. Lett.* **100** 177005
[39] Hwang J 2011 *Phys. Rev.* B **83** 014507
[40] Götze W and Wölfle P 1972 *Phys. Rev.* B **6** 1226
[41] For a review, see Basov D N and Timusk T 2005 *Mod. Phys. Rev.* **77** 721
[42] Puchkov A V, Basov D N and Timusk T 1996 *J. Phys.: Condens. Matter* **8** 10049
[43] van der Marel D, Molegraaf H J A, Zaanen J, Nussinov Z, Carbone F, Damascelli A, Eisaki H, Greven M, Kes P H and Li M 2003 *Nature* **425** 271
[44] Boris A V, Kovaleva N N, Dolgov O V, Holden T, Lin C T, Keimer B and Bernhard C 2004 *Science* **304** 708
[45] Hwang J, Timusk T and Gu G D 2004 *Nature* **427** 714
[46] Moriya T and Ueda K 2000 *Adv. Phys.* **49** 555
[47] Abanov A, Chubukov A V and Schmalian J 2003 *Adv. Phys.* **52** 119
[48] Manske D 2004 *Theory of Unconventional Superconductors—Cooper-Pairing Mediated by Spin Excitations—Introduction* (Berlin: Springer)
[49] Eschrig M 2006 *Adv. Phys.* **55** 47
[50] Carbotte J P, Timusk T and Hwang J 2011 *Rep. Prog. Phys.* **74** 066501
[51] Scalapino D J 2012 *Mod. Phys. Rev.* **84** 1383
[52] Munzar D, Bernhard C and Cardona M 1999 *Physica* C **312** 121
[53] Carbotte J P, Schachinger E and Basov D N 1999 *Nature* **401** 354
[54] Abanov A, Chubukov A V and Schmalian J 2001 *Phys. Rev.* B **63** 180510(R)
[55] Cásek P, Bernhard C, Humlíček J and Munzar D 2005 *Phys. Rev.* B **72** 134526
[56] Chaloupka J and Munzar D 2007 *Phys. Rev.* B **76** 214502
[57] Several features occurring in the mid-infrared range have been interpreted in terms of the GW version of the spin fluctuation model, see, e.g., Basak S, Das T, Lin H, Nieminen J, Lindroos M, Markiewicz R S and Bansil A 2009 *Phys. Rev.* B **80** 124520
Markiewicz R S, Das T and Bansil A 2012 *Phys. Rev.* B **86** 024511
[58] Monthoux P and Pines D 1993 *Phys. Rev.* B **47** 6069
[59] Dahm T, Hinkov V, Borisenko S V, Kordyuk A A, Zabolotnyy V B, Fink J, Büchner B, Scalapino D J, Hanke W and Keimer B 2009 *Nat. Phys.* **5** 217
[60] Marsiglio F, Startseva T and Carbotte J P 1998 *Phys. Lett.* A **245** 172
[61] Chan M K *et al* 2014 arXiv:condmat/1402.4517
[62] Vishik I M *et al* 2014 *Phys. Rev.* B **89** 195141
[63] Li Y *et al* 2012 *Phys. Rev. Lett.* **108** 227003
[64] Homes C C, Tu J J, Li J, Gu G D and Akrap A 2013 *Sci. Rep.* **3** 3446
[65] Ferrell R A and Glover R E 1958 *Phys. Rev.* **109** 1398
[66] Tinkham M and Ferrell R A 1959 *Phys. Rev. Lett.* **2** 331
[67] Emery V J and Kivelson S A 1995 *Nature* **374** 434
[68] Corson J, Mallozzi R, Orenstein J, Eckstein J N and Bozovic I 1999 *Nature* **398** 221
[69] Bilbro L S, Aguilar R V, Logvenov G, Pelleg O, Bozovic I and Armitage N P 2011 *Nat. Phys.* **7** 298
[70] Grbić M S, Požek M, Paar D, Hinkov V, Raichle M, Haug D, Keimer B, Barišić N and Dulčić A 2011 *Phys. Rev.* B **83** 144508
[71] Bilbro L S, Valdés Aguilar R, Logvenov G, Bozovic I and Armitage N P 2011 *Phys. Rev.* B **84** 100511(R)
[72] de Mello E V L 2012 *Europhys. Lett.* **99** 37003
[73] Franz M and Millis A J 1998 *Phys. Rev.* B **58** 14572
[74] Eckl T and Hanke W 2006 *Phys. Rev.* B **74** 134510
[75] Manske D, Dahm T and Bennemann K 2001 *Phys. Rev.* B **64** 144520
[76] Tanaka K *et al* 2006 *Science* **314** 1910
[77] Allen P 1971 *Phys. Rev.* B **3** 305
[78] Allen P B 2004 arXiv:condmat/0407777
[79] van Heumen E, Meevasana W, Kuzmenko A B, Eisaki H and van der Marel D 2009 *New J. Phys.* **11** 055067
[80] van Heumen E, Muhlethaler E, Kuzmenko A B, Eisaki H, Meevasana W, Greven M and van der Marel D 2009 *Phys. Rev.* B **79** 184512
[81] Eschrig M and Norman M 2003 *Phys. Rev.* B **67** 144503 and references therein
[82] Dressel M and Grüner G 2002 *Electrodynamics of Solids: Optical Properties of Electrons in Matter* 2002 (Cambridge: Cambridge University Press)
[83] Degiorgi L, Dressel M, Schwartz A, Alavi B and Grüner G 1996 *Phys. Rev. Lett.* **76** 3838
[84] Millis A J, Zimmers A, Lobo R P S M, Bontemps N and Homes C C 2005 *Phys. Rev.* B **72** 224517
[85] Lucarelli A, Dusza A, Pfuner F, Lerch P, Analytis J G, Chu J H, Fischer I R and Degiorgi L 2010 *New J. Phys.* **12** 073036
[86] Valenzuela B, Nicol E J and Carbotte J P 2005 *Phys. Rev.* B **71** 134503
[87] Fujita K *et al* 2014 *Proc. Natl Acad. Sci. USA* **111** E3026
[88] van Heumen E *et al* 2007 *Phys. Rev.* B **75** 054522